SCIENCE CHINA
Earth Sciences

•ARTICLE•

January 2024 Vol.67 No.1: 234–251
https://doi.org/10.1007/s11430-022-1183-4

A lunar time scale from the perspective of the Moon's dynamic evolution

Dijun GUO[1], Jianzhong LIU[2,10*], James W. HEAD[3], Fuqin ZHANG[4], Zongcheng LING[5,10], Shengbo CHEN[6], Jianping CHEN[7], Xiaozhong DING[8], Jinzhu JI[9] & Ziyuan OUYANG[2]

[1] *State Key Laboratory of Space Weather, National Space Science Center, Chinese Academy of Sciences, Beijing 100190, China;*
[2] *Center for Lunar and Planetary Sciences, Institute of Geochemistry, Chinese Academy of Sciences, Guiyang 550081, China;*
[3] *Department of Earth, Environmental and Planetary Sciences, Brown University, Providence RI 02912, USA;*
[4] *Institute of Geology and Geophysics, Chinese Academy of Sciences, Beijing 100029, China;*
[5] *Shandong Provincial Key Laboratory of Optical Astronomy and Solar-Terrestrial Environment, Institute of Space Sciences, Shandong University, Weihai 264209, China;*
[6] *College of Geoexploration Science and Technology, Jilin University, Changchun 130026, China;*
[7] *School of Earth Sciences and Resources, China University of Geosciences, Beijing 100083, China;*
[8] *Institute of Geology, Chinese Academy of Geological Sciences, Beijing 100037, China;*
[9] *School of Resources and Environmental Engineering, Inner Mongolia University of Technology, Hohhot 010051, China;*
[10] *Center for Excellence in Comparative Planetology, Chinese Academy of Sciences, Hefei 230026, China*

Received September 13, 2022; revised July 2, 2023; accepted September 4, 2023; published online December 15, 2023

Abstract A geologic time scale is a chronological system that separates the geological strata of a planetary body into different units in temporal sequence and shows its progressive evolution. The time scale of the Moon was established a half-century ago during the telescopic-early Apollo exploration era, using data with limited spatial coverage and resolution. The past decades have seen a wide array of studies, which have significantly extended our understanding of global lunar geologic evolution. Based on a comprehensive review of lunar evolution with respect to the dynamical changes, we propose two major updates to the current lunar time scale paradigm to include the evolution of both endogenic and exogenic dynamic forces now known to have influenced early lunar history. Firstly, based on the temporal interplay of exogenic and endogenic processes in altering the Moon, we defined three Eon/Eonothem-level units to represent three dynamical evolutionary phases. Secondly, the pre-Nectarian System is redefined and divided as the magma ocean-era Magma-oceanian System and the following Aitkenian System beginning with the South Pole-Aitken basin. The ejecta of this basin, Das Formation, was deposited on the primordial lunar crust as the oldest stratum produced from exogenic processes. The updated lunar time scale, facilitated by the post-Apollo exploration and research advances, provides an integrated framework to depict the evolution of the Moon and has important implications for the geologic study of other terrestrial planets.

Keywords The Moon, Geologic time scale, Evolution history, Endogenic process, Exogenic process

Citation: Guo D, Liu J, Head J W, Zhang F, Ling Z, Chen S, Chen J, Ding X, Ji J, Ouyang Z. 2024. A lunar time scale from the perspective of the Moon's dynamic evolution. Science China Earth Sciences, 67(1): 234–251, https://doi.org/10.1007/s11430-022-1183-4

1. Introduction

The lunar time-scale plays a fundamental role in geological studies of the Moon and is the foundation for geological maps, which are compiled using basic terrestrial stratigraphic principles (the law of superposition and cross-cutting relationships) (Shoemaker and Hackman, 1962; Wilhelms et al., 1987; Hiesinger and Tanaka, 2020). Meanwhile, lunar

* Corresponding author (email: liujianzhong@mail.gyig.ac.cn)

geologic processes and strata differ from those of the Earth in many ways. Biological fossils, often used as age signatures of terrestrial biostratigraphic system (Gradstein et al., 2020), are absent on the Moon, and the near-vacuum and anhydrous surface environment of the Moon cannot support eolian and fluvial processes, important in sculpturing the surface of the Earth. Additionally, the Moon does not have plate tectonics, which causes tremendous influences on Earth's crust. Instead, the lunar surface is characterized by dense and superposed impact craters with diameters ranging from micrometers to thousands of kilometers (Hörz et al., 1975; Head et al., 2010; Wang et al., 2021). Consequently, the absence of plate tectonics and eolian and fluvial erosion on the Moon makes it possible for the lunar crust/lithosphere to preserve the imprints of the most ancient Earth-Moon system evolution, a record almost entirely obliterated on Earth. Thus, identifying lunar features, strata, and events formed in the earliest lunar history, and providing a stratigraphic framework for reconstructing lunar evolution, are very important for deciphering the early space environment of the Earth-Moon system and early Solar System history.

The present lunar time scale (Wilhelms et al., 1987) was initially defined on the basis of telescopic observations of the lunar nearside and photogeological mapping of the Imbrium and Copernicus region prior to Apollo missions (Shoemaker and Hackman, 1962; Schmitt et al., 1967). After several modifications (Shoemaker, 1964; McCauley, 1966; Wilhelms, 1970; Stuart-Alexander and Wilhelms, 1975), the final form was defined and systematically explained by Wilhelms et al. (1987), using data from Lunar Orbiter and Apollo missions (Shoemaker and Hackman, 1962; Wilhelms, 1970; Wilhelms et al., 1987). The time scale includes five Periods divided by the deposits and characteristics of four impact events, after which the Periods are named, i.e., pre-Nectarian, Nectarian (Nectaris basin), Imbrian (Imbrium basin), Eratosthenian (Eratosthenes crater), and Copernican (Copernicus crater) (Wilhelms et al., 1987). The Imbrian Period is further divided into two Epoch units at the Orientale impact basin event (Wilhelms et al., 1987). This time scale scheme, though based on the nearside geologic evolution, provides a timeline of the most important lunar evolution events including basin-formation impacts, mare basalt eruptions, and ray crater impacts. The principle of using impact ejecta and volcanic deposits as the strata to create lunar stratigraphic system, as employed by Wilhelms et al. (1987), sets an example for the stratigraphic studies of other extraterrestrial planets (Hiesinger and Tanaka, 2020). The particular age dating methods of the Moon, such as crater degradation state and crater size-frequency distribution (CSFD), which were widely used in creating lunar time scale (Wilhelms et al., 1987), have been general ways to define relative ages on the Moon and Mars, and the latter can also be used to estimate absolute ages.

The current time-scale was developed when the exploration and analysis of the Moon were in their early stages. Although it has served lunar geoscience community over the past decades, its shortcomings are obvious and widely discussed (Stoffler et al., 2006; Hiesinger and Tanaka, 2020). The areal coverage and spatial resolution of the collected data could not support detailed global-scale studies (Shoemaker, 1964; McCauley, 1966; Wilhelms, 1970; Stuart-Alexander and Wilhelms, 1975), and early optical-wavelength remote-sensing instruments precluded a more detailed definition and characterization of geological units that would become common with a wider range of data (Head et al., 1978). Motivated by the sample-return tasks during Apollo and Luna missions, the nearside of the Moon was explored and studied in great detail and its stratigraphic system provides the foundation of the time scale scheme (Shoemaker and Hackman, 1962; Stuart-Alexander and Wilhelms, 1975; Wilhelms, 1970; Wilhelms et al., 1987). Thus, the time-scale generally fails to do justice to a global perspective nor give equal consideration to the farside, where the terranes are more ancient and primordial (Jolliff et al., 2000). The events employed as stratigraphic markers of the time scale were all occurred in the nearside, though the farside South-Pole Aitken (SPA) basin created the largest ejecta stratum of the Moon (Petro and Pieters, 2008). In addition, the time-scale focuses on specific impact events in defining units, whereas early endogenic processes, particularly the formation and evolution of the magma ocean and primary crust (Taylor, 1989), were not sufficiently reflected (Wilhelms et al., 1987). Due to the absence of definitive rock-stratigraphic units, the stratigraphic boundaries of the Imbrian-Eratosthenian and Eratosthenian-Copernican are subject to interpretation and debate (Stoffler et al., 2006; Hiesinger and Tanaka, 2020). The pre-Nectarian Period, defining the earliest period of lunar history, includes two phases of lunar dynamic evolution, i.e., magma ocean formation and solidification (endogenic) and the numerous large impact basins (exogenic), beginning with the SPA basin (Wilhelms et al., 1987; Elkins-Tanton et al., 2011; Norman and Nemchin, 2014).

Since the end of the Apollo program, lunar science has benefitted from new missions, new technologies, and new perspectives on the history of the Moon, particularly its formative years and early evolution. Understanding of the formation of the Moon and the nature and evolution of endogenic processes (e.g., magma ocean differentiation, volcanism) have significantly improved through remote sensing observations (Hiesinger et al., 2010; Morota et al., 2011; Gustafson et al., 2012; Whitten and Head, 2015; Qiao et al., 2017), laboratory analyses (Neal and Taylor, 1992; Borg et al., 1999, 2015; Elkins-Tanton et al., 2011; Weiss and Tikoo, 2014), and numerical simulations (Stegman et al., 2003; Laneuville et al., 2018; Maurice et al., 2020). Exogenic processes, specifically, impact cratering, have been in-

vestigated in detail through impact crater mapping (Head et al., 2010; Neumann et al., 2015; Povilaitis et al., 2018; Robbins, 2019; Wang et al., 2021; Huang et al., 2022), cratering experiments and simulations (Holsapple, 1993; Schultz et al., 2011; Collins et al., 2012, 2020; Johnson et al., 2016; Schultz and Crawford, 2016; Melosh et al., 2017), and impactor flux estimations (Gomes et al., 2005; Boehnke and Harrison, 2016; Bottke and Norman, 2017; Conrad et al., 2018; Morbidelli et al., 2018; Nesvorný and Roig, 2018; Mazrouei et al., 2019; Zhu et al., 2019a). These advances make it possible to assess the evolution of the Moon in a more holistic and synergistic manner. Additionally, one of the most important aspects of this progress has been the recognition of the role of the SPA basin in lunar history and evolution (Jolliff et al., 2000; Petro and Pieters, 2008; Garrick-Bethell and Zuber, 2009; Schultz et al., 2011; Melosh et al., 2017; Moriarty and Pieters, 2018). As the largest and oldest impact structure confidently recognized on the Moon (Garrick-Bethell and Zuber, 2009; Orgel et al., 2018), the SPA basin exerted a significant influence on the lunar surface, crust, and lithosphere, creating a unique terrane (Jolliff et al., 2000; Petro and Pieters, 2008; Schultz et al., 2011; Melosh et al., 2017), and marking a turning point in lunar evolution.

In order to help provide a more holistic and synergistic framework of lunar history, we carried out a comprehensive analysis of lunar geologic evolution with respect to the nature and relationship of dynamical changes, i.e., endogenic and exogenic evolution. Utilizing the wealth of overviewed information, we describe a three-phase pattern of dynamical evolution, based on which we propose three Eon/Eonothem-level units in the context of the current lunar time-scale. We divided the pre-Nectarian Period into two Periods with the boundary defined at the SPA basin. We identified the rock-stratigraphic unit composed by the ejecta deposit of the SPA basin and formulate a stratigraphic column corresponding to the modified time scale.

2. Dynamic evolution of the Moon

2.1 Nature and evolution of lunar endogenic processes

Endogenic processes (e.g., core-mantle-crust formation and evolution, magmatism resulting in intrusion and extrusion, heat transfer and loss with time) that played a fundamental role in early evolution of the Moon (Taylor, 1989; Shearer et al., 2006; Hiesinger et al., 2010; Elkins-Tanton et al., 2011; Whitten and Head, 2015) were the major forces in lunar crustal formation and the resulting major crustal provinces (Jolliff et al., 2000). According to the giant impact theory, the Moon was formed through an impact on the primordial Earth at ~4.52–4.50 Ga (Lee et al., 1997; Canup, 2012; Barr, 2016; Lock et al., 2018). After an accretion of hundreds of years following the giant impact (Salmon and Canup, 2014; Sahijpal and Goyal, 2018), the initial Moon was covered with molten magma (as deep of many hundreds of kilometers), known as lunar magma ocean (LMO) (Wood, 1975; Warren, 1985; Elkins-Tanton et al., 2011). Cooling of the LMO created the initial structure of the Moon, separating out the primary primordial anorthositic flotation crust. Chronologic studies on ferroan anorthosite (FAN) of the returned samples have produced varying ages of the crust of the Moon, ranging from older than 4.4 Ga (Borg et al., 2015) to the youngest 4.29 Ga (Borg et al., 1999), spanning a duration of over 150 million years (Figure 1c). Such a prolonged magma ocean was unexpected, while numeric simulation shows that it could be sustained due to the high insulating efficiency of the anorthositic crust (Maurice et al., 2020). Through systematic isotopic analysis, Boyet et al. (2015) pointed out that the lunar FANs are from different sources and some of them may not be the primary product of the LMO. As a consequence of impact cratering and volcanic processes, the primordial crust was fractured to form the megaregolith (Richardson and Abramov, 2020) and the lithology has become more complex due to mixture of excavated deep material and filling of mare basalts in floor of large craters (Hiesinger et al., 2011). With global remote sensing investigation, the primary anorthositic crustal material has been identified at some outcrops due to the late impact excavation processes (Ohtake et al., 2009; Yamamoto et al., 2012). Following formation of the primary crust (Taylor, 1989), magmatic process continued through the form of intrusions (Shearer et al., 2006); the presence of plutonic rocks, such as the magnesian suite and alkali suite observed in Apollo samples (Figure 1c), indicates that the non-mare intrusive magmatism persisted until ~4.0 Ga (Snyder et al., 1995; Shearer et al., 2006; Borg et al., 2015).

Mare basalts, which filled in ancient impact craters, basins, and low-lying areas, are the most prominent extrusive endogenic products on the lunar surface, covering ~17% of lunar surface and concentrated on the nearside (Head and Wilson, 1992). The Apollo samples show that mare eruptions were very active during ~4.0–3.1 Ga (Snape et al., 2019) (Figure 1). Model ages of the basaltic units based on CSFD analyses suggest that the maria were emplaced from ~3.9 Ga to ~1.2 Ga with a steep rise at ~3.55 Ga, but the eruption rapidly decreased at 3.0 Ga (Figure 1a), and no present activity is known (Hiesinger et al., 2011; Snape et al., 2019). The latest Chang'e-5 mission returned the youngest mare basalt samples, which verified the late volcanism at ~2 Ga (Che et al., 2021; Li et al., 2021). Remote sensing investigations suggest that the late mare eruptions were much weaker than the Imbrian Period (Morota et al., 2011). In addition to the exposed mare basalts, the cryptomare underlie areas of subsequent crater ejecta deposits indicates that mare volcanism could start much earlier (Whitten and Head, 2015). The identified cryptomare units supply ~1.8% addi-

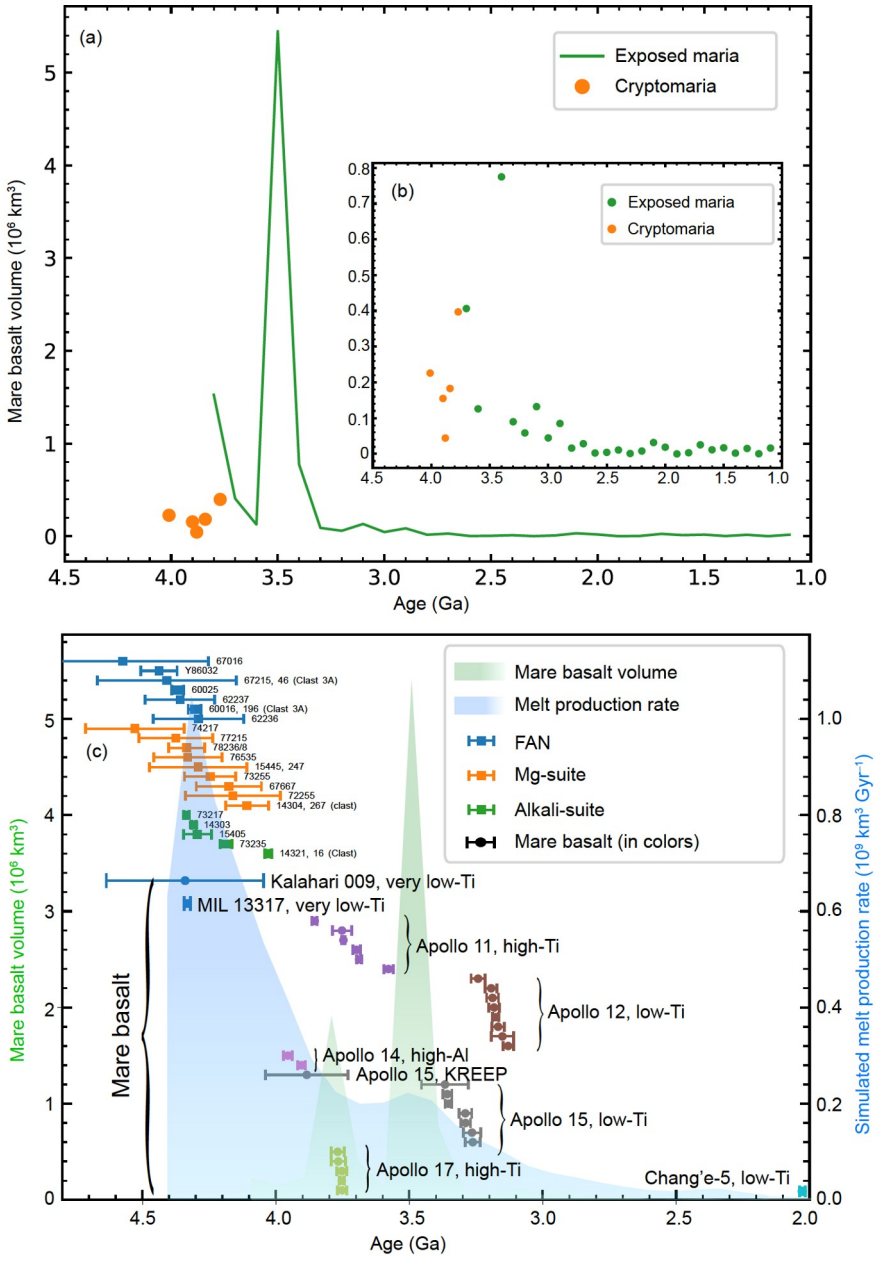

Figure 1 (a) Estimated volume of exposed maria (green) and cryptomaria (orange) erupted in the history of the Moon. The inset diagram (b) shows the data truncated at the volume of 0.8×10^6 km^3 to better illustrate the data with small values. For the cryptomaria, only those with continuous areas ≥20,000 km^2 are considered to ensure robust age estimates (Whitten and Head, 2015). (c) The evolution of mare basalt volume and simulated melt production rate, along with ages of lunar samples produced in different endogenic processes. The melt production rate is based on the model 5 simulation of Laneuville et al. (2018) with nearside-farside averaged. The volume of mare basalts includes both exposed maria and identified cryptomaria (Hiesinger et al., 2011; Whitten and Head, 2015). The ages of ferroan anorthosite (FAN), Mg-suite, and Alkali-suite are from Borg et al. (2015), Marks et al. (2019), and Gross and Joy (2016). The mare basalt age data include those from meteorites (Terada et al., 2007; Curran et al., 2019), Apollo samples (Snape et al., 2019), and Chang'e-5 samples (Li et al., 2021; Li et al., 2022). Note that the sample ages are displayed with vertical offset for clarity purposes and do not correspond to either of the vertical axis values.

tional mare basalt area, and extend the oldest mare eruption from ~3.77 Ga to ~4.01 Ga (Figure 1a) (Whitten and Head, 2015). Lunar meteorites Kalahari 009 and basalt clasts from Miller Range (MIL) 13317 suggest that mare volcanism may have commenced as early as ~4.35 Ga (Terada et al., 2007; Curran et al., 2019) (Figure 1c). Thus, the earliest volcanic materials could be admixed in the megaregolith due to impact processes. With the continued conductive cooling of the Moon, internal energy ultimately became insufficient to support any additional large-scale volcanic activity and the endogenic processes have declined since the Eratosthenian Period (3.16–0.8 Ga) (Wilhelms et al., 1987; Hiesinger et al., 2011; Morota et al., 2011; Laneuville et al., 2013; Yue et al., 2017), as shown in Figure 1c. Based on the concentration of

TiO_2, mare basalts can be categorized as different groups (Neal and Taylor, 1992), and Apollo basalt samples indicate that older mare basalts are more enriched with TiO_2 (Nyquist and Shih, 1992), as shown in Figure 1c. However, lunar meteorites show that the oldest lunar basalts may have the lowest TiO_2 and highest Al_2O_3 contents (Curran et al., 2019) (Figure 1c).

Though rich information from lunar samples and remote sensing observations, the nature and magnitude of internal processes are difficult to quantify through direct observations, and thus thermal modeling is usually employed to characterize the process (Laneuville et al., 2018; Sahijpal and Goyal, 2018). Laneuville et al. (2018) simulated the early thermal history of the Moon and the melt production rate, which provides a measure of the level ("intensity") of endogenic activity (Figure 1c). The simulations indicated that the magmatic activities and melt production rate of the Moon were intense and high in the first billion years and declined at ~3 Ga (Laneuville et al., 2018). Additional evidence supporting vigorous endogenic energy in early lunar history is paleomagnetism. Apollo sample measurements indicate that a global magnetic field was generated by an ancient lunar core dynamo, which had an intensity comparable to present Earth during the 4.25–3.56 Ga period, but rapidly declined after ~3.3 Ga (Mighani et al., 2020; Stegman et al., 2003; Weiss and Tikoo, 2014).

2.2 Nature and evolution of lunar exogenic processes

The Moon has been dominated by two types of exogenic processes since the formation of the solidified crust: impact cratering and space weathering. Here we mainly assess impact processes, as space weathering only influences the superficial regolith and has little effect on the crust and lithosphere of the Moon. Impact craters on the Moon have a wide size range, from micrometers to thousands of kilometers (Hörz et al., 1975; Head et al., 2010; Wang et al., 2021); a crater of diameter ⩾300 km is generally called an impact basin (Wilhelms et al., 1987). Some craters diameter in 200–300 km are also categorized as basins in a few cases (e.g., Baker et al., 2017; Liu et al., 2022). We employed the classic definition of basins due to more information of their formation ages than small craters and the dominant contribution of impact kinetic energy. The oldest commonly accepted impact basin is the South Pole-Aitken basin, dated as ~4.2–4.3 Ga based on crater counting (Hiesinger et al., 2012; Orgel et al., 2018; Povilaitis et al., 2018). This age is consistent with the basin-scale impact events recorded in Apollo samples 67955 (Norman and Nemchin, 2014) and 76535 (Garrick-Bethell et al., 2020; White et al., 2020). The SPA impact event marks the first recorded and preserved exogenic activity on lunar lithosphere when the lunar primordial crust became rigid enough. With a diameter of ~2400 km (Garrick-Bethell and Zuber, 2009), the SPA basin is also the largest confirmed impact basin on the Moon (some consider the nearside "Procellarum Basin" larger and earlier (Whitaker, 1981; Zhu et al., 2019b), but this is not universally accepted). The consequence of this giant impact might lead to the compositional asymmetry of the Moon (Jones et al., 2022; Zhang et al., 2022). Ejecta of the SPA impact were widespread enough such that it could obliterate all the previous geological surface morphologic imprints (Petro and Pieters, 2008). This event was followed by 42 additional basin-scale impacts (Wilhelms et al., 1987; Orgel et al., 2018), terminating at the Orientale impact event. Formation of the Orientale basin marks the general end of the heavy bombardment period; with the declining flux, craters formed subsequently are smaller in size.

The magnitude of an impact event can be characterized with the kinetic energy of the impactor and the impactor size can be derived from crater size with scaling laws (Appendix eq. (S1), https://link.springer.com). In impact events, the kinetic energy increases as the third power to increasing impactor size at the same impact velocity. (eqs. (S2) and (S3)). An impactor of 10 times in size carries more than 1000 times of kinetic energy (Appendix Figure S1). Therefore, we only considered the kinetic energy of the craters with diameter greater than 10 km in this work. The sizes and ages of 43 basins with diameters greater than 300 km are adopted from previous studies (Petro and Pieters, 2008; Orgel et al., 2018). Because old craters are heavily degraded and diminished and most of the identified lunar craters are not dated, the size-frequency of craters diameter in 10–300 km is modeled through crater production function described in (Neukum et al., 2001). The calculation assumed an average velocity of 19.7 km s^{-1} with an impact angle of 45 degrees from the surface (Le Feuvre and Wieczorek, 2008). As shown in Figure 2, the impact kinetic energy was extremely high during ~3.8–4.3 Ga, the period when dozens of basins were created. After the Orientale basin impact (~3.8 Ga), impact energy rapidly declined and has remained a relatively low and constant impact rate and magnitude since ~3 Ga (Figure 2). At the beginning of the Eratosthenian Period (~3.2 Ga), the impact energy was only a factor of 0.0003 of the average value during the Nectarian Period. In practice, the Eratosthenian and Copernican craters can be distinguished by the radial bright features of the ejecta, which decay and darken with effects of space weathering (Wilhelms et al., 1987). Copernican craters are young enough to preserve the ray systems, while those of Eratosthenian craters have degraded.

3. Updating of lunar time scale scheme

Throughout the evolution history of the Moon, the impact of

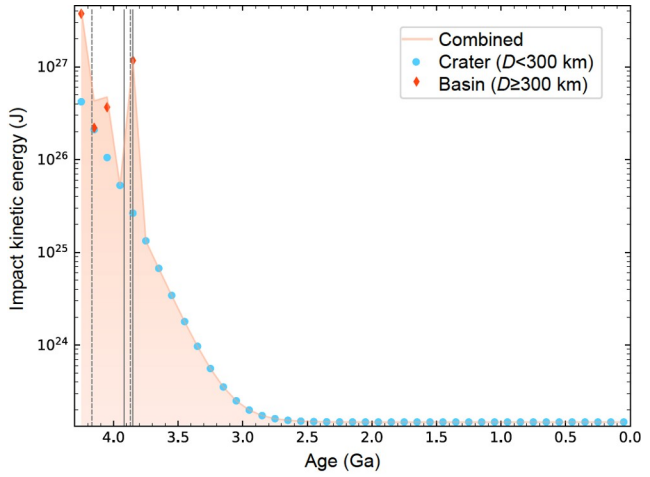

Figure 2 The evolution of lunar exogenic power that is indicated by impact kinetic energy. The shadowed area shows the impactor kinetic energy of all the craters with diameter larger than 10 km. The blue point shows the impactor kinetic energy of craters with diameter in the range of 10–300 km, where the crater size-frequency distribution is based on differential lunar crater production rate. The red diamond shows the impactor kinetic energy of basins ($D \geqslant 300$ km). The interval of kinetic statistics is 0.1 Ga. The solid vertical lines represent the beginning of the Nectarian (3.92 Ga) and Imbrian (3.85 Ga) based on Wilhelms et al. (1987) and Neukum and Ivanov (1994). The dashed vertical lines represent the model ages of the Nectaris basin (4.17 Ga) and Imbrium basin (3.87 Ga) according to Orgel et al. (2018).

endogenic and exogenic forces has varied in terms of their respective contributions across different geological time periods. The melt production rate (Laneuville et al., 2018) and the estimated volume of mare basalts (Hiesinger et al., 2011; Whitten and Head, 2015) are reflections of the thermal state of the lunar interior, which is a measure of the magnitude of endogenic process and their evolution. The magnitude of lunar exogenic process is represented by the evolution of impact kinetic energy. The evolution of the two types of processes, as a function of time, is shown in Figure 3, together with the samples recording different processes.

As shown in Figure 3, the Moon's history can be divided into three evolutionary phases defined on the basis of the influence and effects of endogenic and exogenic processes. The first phase specifically refers to magma ocean formation, differentiation and the solidification of the primary crust (Taylor, 1989), a phase of evolution that largely involved endogenic forces and processes (Figure 3). Before the lunar crust was solidified to rigid enough, the kinetic energy of impactors was transformed into internal energy associated with the magma ocean (Perera et al., 2018). The pre-SPA impacts might not have left any morphologic or stratigraphic records due to the thermal structure and crustal/lithospheric relaxation processes (Perera et al., 2018). Even if topographic evidence had been created, it was very likely to be covered and obliterated by the globally emplaced SPA ejecta (Petro and Pieters, 2008). The SPA impact event marks the onset of the next phase in lunar evolution, during which impact cratering started to play an increasingly important role in changing the topography and structure of lunar lithosphere (Figure 3). It is noteworthy that the SPA impact does not necessary to be just right at the end point of the crustal solidification, and the LMO could terminate earlier or later than this event. The ejecta deposits of large craters such as the impact basins created chronostratigraphic markers recognizable at local, regional, and global scales (Wilhelms et al., 1987; Hiesinger and Tanaka, 2020). Despite the alterations caused by subsequent cratering processes, the structure and stratigraphic record of the SPA basin have been able to be preserved owing to its vast dimensions. In the cratering processes, the size and energy of the great impacts fractured lunar crust, excavated huge volumes of material, uplifted isotherms, and significantly reduced crustal thickness in the basin interior, factors which are favorable to the eruption and accumulation of mare basalts. The related igneous and volcanic activity (Head and Wilson, 1992; Shearer et al., 2006; Borg et al., 2015; Head and Wilson, 2017) indicate that endogenic processes were also prominent in the basin-forming period and the subsequent billion years (Figure 3). In summary, the second evolutionary phase was controlled by both endogenic and exogenic forces, which lasted until ~3.1–3.3 Ga (Figure 3), corresponding to the boundary between the Imbrian and Eratosthenian Periods (Wilhelms et al., 1987). Though late volcanism has been identified from remote sensing (Morota et al., 2011) and returned samples (Che et al., 2021; Li et al., 2021), the scales are believed to be much smaller than earlier eruptions (Figure 1a). Moreover, the last eruption is hard to be identified and dated at present time. The third phase thus started at about 3 Ga, from which time endogenic forces waned and gradually ceased with the decaying lunar interior energy sources (Figure 3). In the third phase, the Moon enters a relative quiescence status without substantial endogenic activity (Hess and Parmentier, 1995; Hiesinger et al., 2012; Whitten and Head, 2015; Laneuville et al., 2018), and the lunar surface is locally modified mainly by impact events, though the craters are significantly smaller than earlier basins (Wilhelms et al., 1987). Exogenic processes thus dominate over endogenic processes in the third evolutionary phase of the Moon.

From the perspective of geoscience, the phased evolution of the Moon described above can be seen as a key component in defining the geologic time scale. Chronostratigraphic (or time-stratigraphic) units (e.g., Eonothem, System) and geochronologic (or time) units (e.g., Eon, Period) are two categories of the time scale units (Salvador, 2013). Chronostratigraphic units are bodies of rocks defined between specified stratigraphic horizons which represent specified intervals of geologic time, and geochronologic units are the geologic time during which chronostratigraphic units were formed (Salvador, 2013). From a geochronologic per-

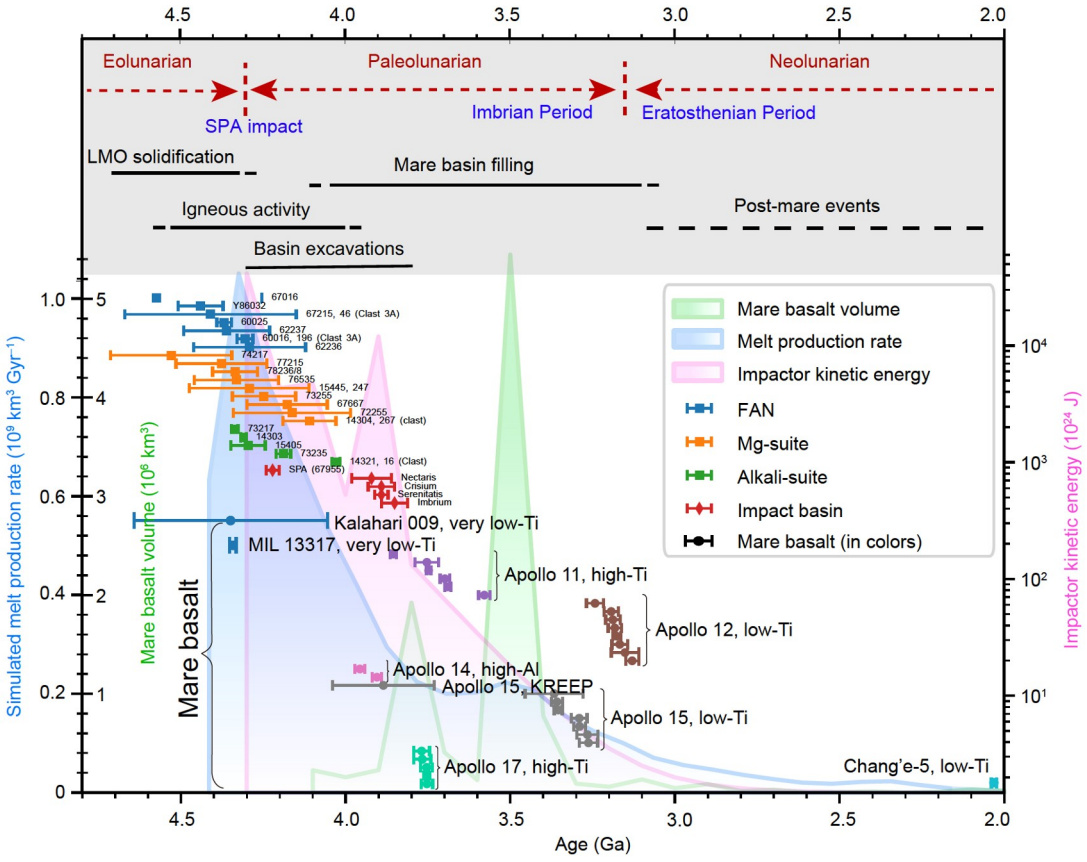

Figure 3 The evolution of lunar endogenic and exogenic processes and the resulting three dynamical phases being designated as Eolunarian, Paleolunarian, and Neolunarian from old to young. In addition to the sample data shown in Figure 1c, the ages of samples representing basin formation events (Stoffler et al., 2006) are also displayed. Evolution of endogenic processes (indicated by simulated melt production rate and mare basalt volume) and exogenic processes (indicated by impactor kinetic energy) are shown as shaded curves. Note that the sample ages are displayed with vertical offset for clarity purposes and do not correspond to any of the vertical axis values.

spective, the three phases of lunar dynamic evolution can be treated as three units of the time scale. Referring to the principles of the International Commission on Stratigraphy (ICS) (Remane et al., 1996; Gradstein and Ogg, 2020), the chronostratigraphic chart and time scale of the Earth (Cohen et al., 2013; Gradstein et al., 2020), as well as the current lunar time scale (Wilhelms et al., 1987; Zhang et al., 2010), we propose to define three time scale units and conveniently be designated: Eolunarian, Paleolunarian, and Neolunarian, subdivisions at the level of Eon/Eonothem (Figure 3; Table 1). The three Eon/Eonothem units would thus constitute the highest level of the lunar time scale. However, they cannot be readily fit to the Period/System level units defined in the time scale of Wilhelms et al. (1987). The pre-Nectarian Period of Wilhelms et al. (1987) consists of both the magma ocean evolution period and impact events of tens of basins, which correspond to the Eolunarian and Paleolunarian, respectively. The SPA basin marks the turning point from the endogenic-dominated phase to the phase when endogenic and exogenic processes were comparable in reshaping the lunar crust and lithosphere. Thus, we divide the pre-Nectarian Period into two Periods with the boundary defined by the SPA basin (Table 1). The older Period, which begins with the formation of the Moon and ends at the SPA impact event, is occupied by the magma ocean era and thus is named as the Magma-oceanian (Mo in short) Period/System, which is the only Period in the Eolunarian Eon (Table 1). The next younger period, which begins with the SPA basin formation and lasts to the lower boundary of the Nectarian Period, could be designated the South Pole-Aitkenian Period by convention (Wilhelms et al., 1987), but such a long name is complex and inconvenient. We thus suggest that it be designated as Aitkenian Period because the Aitken crater, which is the northern endpoint of the SPA basin, is a landmark for the giant basin and part of the original name of the basin. The lower time boundary of the Aitkenian Period is assigned as 4.31 Ga adopted from Orgel et al. (2018), but needs to be preciously dated with samples from the SPA basin. A summary of the proposed lunar time scale, highlighting lunar dynamic evolution, is shown in Table 1.

Ages of the defining events and strata are fundamental components in developing a time scale. However, many of these ages are ambiguous and difficult to be resolved without new samples from specific target regions for analysis. The

Table 1 The lunar time scale viewed from the dynamic evolution perspective of the Moon

Geochronologic/chronostratigraphic unit			Major geologic process	Age (Ga)
Neolunarian (NL) Eon/Eonothem	Copernican (C) Period/System		Impacts to form the young craters with recognizable ray system	0.0 0.8
	Eratosthenian (E) Period/System		Impact crater formation; Small scale mare eruptions	0.8 3.16
Paleolunarian (PL) Eon/Eonothem	Imbrian (I) Period/System	Late Imbrian Epoch/Upper Imbrian Series	Extensive mare eruptions in the floor of ancient basins and large craters; Impact crater formation	3.16 3.8
		Early Imbrian Epoch/Lower Imbrian Series	Impacts of the Imbrium, Orientale, and Schrödinger basin; Magmatism	3.8 3.85
	Nectarian (N) Period/System		Impacts of the Nectaris and subsequent basin before the Imbrium basin; Magmatism	3.85 3.92
	Aitkenian (A) Period/System		Impacts of the SPA and subsequent basin before the Nectaris basin; Magmatism	3.92 4.31
Eolunarian (EL) Eon/Eonothem	Magma-oceanian (Mo) Period/System		Crystallization of the magma ocean and formation of the primary anorthositic lunar crust	4.31 4.52

main challenge lies in linking the absolute age to a specific impact event due to the comminution, migration, and re-melting of impact melt rocks that recorded the formation age. In order to minimize controversy, we have adopted age data based on the comprehensive analysis conducted by Wilhelms et al. (1987) and Stöffler and Ryder (2001). The age of the Nectaris basin is derived from the Apollo 16 samples, specifically the North Ray crater ejecta, which is believed to contain the excavated Nectaris continuous ejecta deposits known as the Descartes Formation (Stöffler and Ryder, 2001). Within the range of 3.84 Ga to 4.14 Ga obtained from the samples, an age of 3.92 Ga has been assigned to the Nectaris basin due to its consistency with the assumed crater production rate (Wilhelms et al., 1987). However, it is also possible that the Descartes Formation could be the ejecta deposits of the younger and larger Imbrium basin (Norman et al., 2010), and the age of the Nectaris basin has also been dated 4.1–4.2 Ga (Fischer-Gödde and Becker, 2011). The age of the Imbrium basin is mainly determined based on the Apollo 14 and 15 samples (Stöffler and Ryder, 2001). The Apollo 14 mission returned samples from the Fra Mauro Formation, the continuous ejecta deposits of the Imbrium basin, and collected impact melt breccias. By landing inside the Imbrium basin near its eastern rim known as the Apennine Mountains, the Apollo 14 mission very likely obtained Imbrium impact melt rocks, enabling the derivation of a robust age. The derived age for the Imbrium basin is ~3.85 Ga (Wilhelms et al., 1987; Stöffler and Ryder, 2001). Although it is straightforward to link the Apollo 14 and 15 samples to the Imbrium basin, other ages have been proposed. The Apollo 17 poikilitic impact melt breccias, which were attributed to the Serenitatis basin, could potentially have originated from the Imbrium basin based on the texture and trace element concentrations of sample 73155, and its weighted mean age is 3921±14 Ma (Zhang et al., 2019). Using various chronological methods, Nemchin et al. (2021) further analyzed the Apollo 14 and 15 impact melt breccias and narrowed the Imbrium impact time to 3922±12 Ma. However, assigning the ages to specific impacts is less certain compared to the derived age value (Nemchin et al., 2021). In addition to radiometric ages, Orgel et al. (2018) utilized the buffered nonsparseness corrected CSFD approach to derive ages of $4.17^{+0.012}_{-0.014}$ Ga for the Nectaris basin and $3.87^{+0.035}_{-0.046}$ Ga for the Imbrium basin. To summarize, it is still too early to definitively determine the ages of these two basins. The age of the Orientale basin is not constraint by any returned samples, and it has been dated as 3.8 Ga based on crater density (Wilhelms et al., 1987; Stöffler and Ryder, 2001), which is consistent with the more recent comprehensive CSFD dating results (Orgel et al., 2018; Yue et al., 2020). The lower boundary age of the Eratosthenian Period is determined by the Apollo 12 mare basalt rocks, which have ages ranging from 3.08 Ga to 3.26 Ga (Wilhelms et al., 1987). An average age of 3.16 Ga has been adopted by Wilhelms et al. (1987). Though Copernicus crater has been dated ~800±15 Ma based on the sampled ejecta material at the Apollo 12 landing area (Wilhelms et al., 1987; Stöffler and Ryder, 2001), many other bright-ray craters are older than Copernicus. Hiesinger and Tanaka (2020) suggests that the lower boundary of the Copernican Period could be between 1.25 and 2.2 Ga if bright rays are used as the criterion.

4. The rock-stratigraphic basis of the Aitkenian Period

As a geologic time-scale unit, it is essential for the newly-defined Aitkenian Period to be assigned with its rock-stratigraphic basis. The ejecta deposits of giant impact basins are commonly treated as rock-stratigraphic units on the Moon, such as the Jansen Formation of the Nectaris basin (Stuart-Alexander and Wilhelms, 1975; Wilhelms et al., 1987) and the Fra Mauro Formation of the Imbrium basin (Wilhelms, 1970; Wilhelms et al., 1987). The lower boundary of the Aitkenian System is the SPA ejecta deposit, even though the original materials (likely to be quite thick, and global in extent) could be difficult to recognize due to post-event geological modification. We defined the stratum by identifying the compositional signatures of excavated mantle materials in the region of interest that suffered from less post-modifications.

4.1 Region of interest for SPA ejecta detection

Three-dimensional impact simulations indicate that the ejecta deposit of the SPA basin at the outer ring were as thick as ~6–8 km, of which material from the mantle may have contributed ~2–5 km (Melosh et al., 2017). Mineralogical analysis interprets the excavated mantle material is dominated by low-calcium orthopyroxene (OPX) (Melosh et al., 2017). As ejecta thickness decreases with increasing distance from the parent impact crater (Melosh et al., 2017), the ejecta are most likely to be preserved and identified at the continuous ejecta facies, located within ~1–1.5 radii from the parent crater rim. The dominant processes modifying SPA ejecta are postdated impacts, which are spatially inhomogeneous especially for the larger impacts that created greater influence on SPA ejecta. Thus, we can define the regions of interest that are less affected by post impacts to locate the area for further investigation. A representative indicator to quantify the relative effect degree of an impact on the target area (outside the crater interior) is the thickness of the deposited ejecta, and a larger thickness of ejecta deposit represents a greater influence. Using the ejecta decay model of equation 12 in Pike (1974), we simulated the ejecta accretion from post-SPA impact craters with diameter greater than 200 km. The transient diameter of the craters was calculated based on the scaling laws of Holsapple (1993).

The simulated ejecta distribution is shown in Figure 4b, which shows that three regions (A, B, and C) have relatively smaller ejecta thickness than the rest of the areas. In these regions, the cumulative ejecta are ≤~350 m, and it could be ≤ ~200 m if simulated with the decay model of Housen et al. (1983). The northern region A is surrounded by concentrated craters and basins greater than 200 km. The southern region C, which is located in the polar region, has poor illumination conditions. The northeastern region B is consistent with the area being discovered with OPX-dominated material (Melosh et al., 2017), and thus was selected as the region of interest. Simulated thickness distribution provides a good constraint to the relative amount of post-SPA ejecta, but the absolute value is less reliable, especially in the discontinuous phase. Though the estimate of accumulated foreign ejecta are 100s meters thick, the material in region B should be dominated with the local material due to the erosion and exhumation processes along with the ballistic ejecta sedimentation. For instance, the ratio of local material to foreign material, based on the empirical function of (Petro and Pieters, 2006), is ~2.0 at the rim of the Korolev basin, which is the smallest basin (diameter in 440 km) around the region B. Therefore, as the investigation area is located in the discontinuous ejecta phase where the primary ejecta were sparsely emplaced and the area is 100s km away from the primary crater rim, we can assume that the local SPA ejecta should be the dominate component of the regolith. Moreover, this region has been widely excavated by craters tens of kilometers in diameter in a history of greater than 3.8 Gyr (after the Orientale impact), which could exhume the buried substrata and increase the proportion of SPA ejecta in the surface regolith.

4.2 Geology and rock-stratigraphic system

4.2.1 Identification of the rock-stratigraphic basis of the Aitkenian Period

Located on the farside highland area with high elevation (Figure 4a), region B and its peripheral terrain are heavily cratered seen from the Lunar Reconnaissance Orbiter (LRO) Wide Angle Camera (WAC) mosaic image (100 m pixel^{-1}) (Figure 4c). Surrounding basins, including the Aitkenian Apollo basin, the Nectarian Korolev basin and Hertzsprung basin, and the Imbrian Orientale basin, have caused significant influences on this area (Figure 4a and 4c). The subregion lying between the Sternfeld and Das craters (referred to as the Sternfeld-Das region) is located beyond continuous ejecta fields of surrounding basins (Figure 4c). The surface of the subregion does not show radial textures related to sedimentation of post-SPA impact ejecta (Figure 4c). The western portion of the Sternfeld-Das region is geologically contacted with ejecta deposits from the Korolev basin and Hertzsprung basin (Figure 4c). Due to being highly degraded, the radial texture of the Korolev basin ejecta is almost indiscernible. The radial texture of the Hertzsprung ejecta is preserved in the continuous facies and the superposition relations suggest that Hertzsprung is younger than Korolev and SPA. However, the Hertzsprung ejecta in the overlapping areas is discontinuous. The ejecta deposit of the Orientale basin, i.e., the Hevelius Formation (Wilhelms et al., 1987), do not show clear evidence in this area due to the

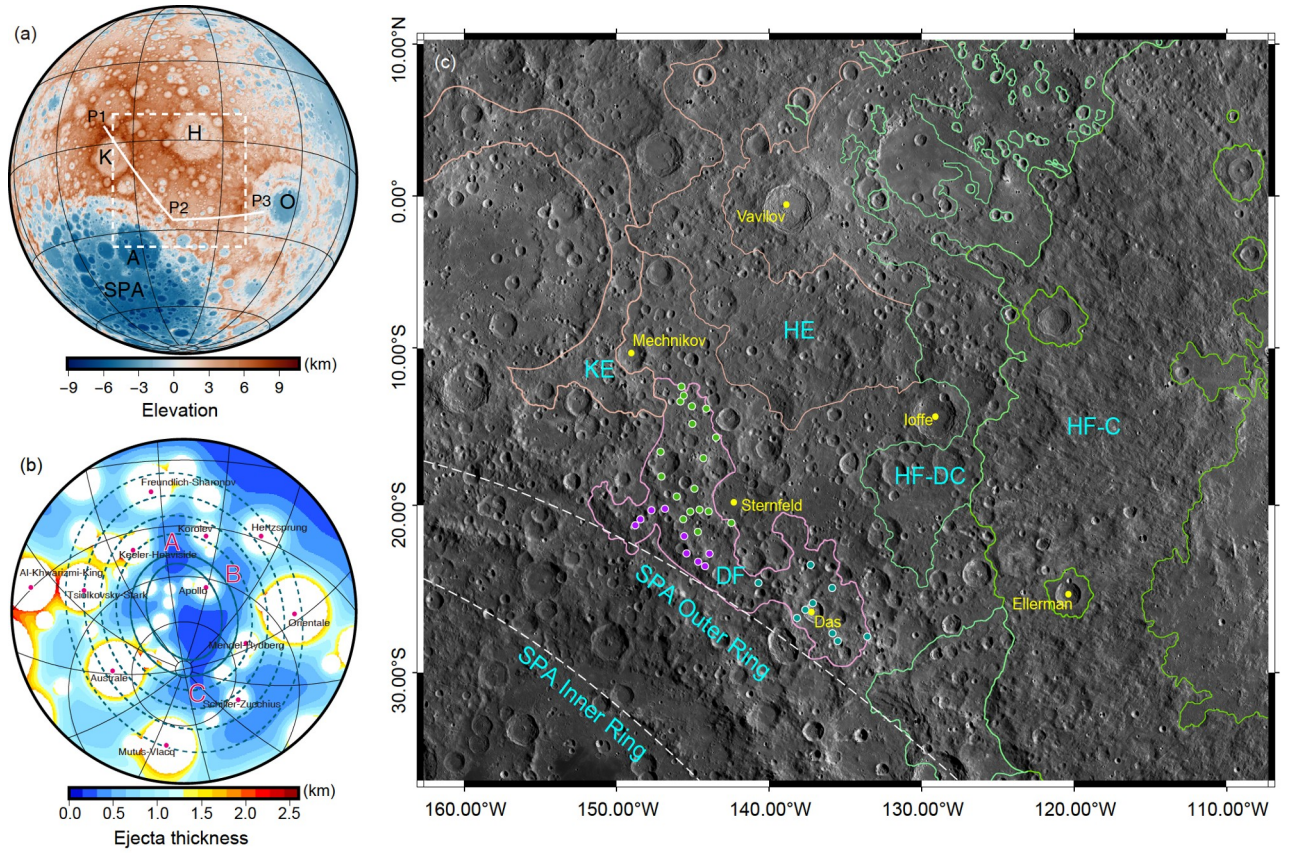

Figure 4 (a) The LRO Lunar Orbiter Laser Altimeter (LOLA) elevation of the Moon in orthographic projection (133.2°W, 13.3°S), where A: Apollo basin, K: Korolev basin, H: Hertzsprung basin, and O: Orientale basin. The white dashed square represents the extent of (c) but are not in strict conformance due to the map projection differences. The solid line P1-P2-P3 represents the trace of the geological cross-section discussed in section 4.2.2. (b) Cumulative ejecta thickness from craters diameter greater than 200 km and younger than the SPA basin, presented in stereographic projection (168.9°W, 53.2°S). The ejecta thickness is calculated with equation 12 of Pike (1974). Crater interiors are filled in white. The three regions where post-SPA ejecta are relatively thin are labeled with A, B and C. The solid dark blue ellipses show the estimated inner ring and outer ring of the SPA basin (Garrick-Bethell and Zuber, 2009). The dashed dark blue lines show annuli with the width of a quarter of the SPA outer ring ellipse axes. (c) The LRO WAC image of the northeast region of the SPA basin presented in Mercator cylindrical projection (133.2°W, 13.3°S), where DF: Das Formation (the Sternfeld-Das region), KE: Korolev basin ejecta, HE: Hertzsprung basin ejecta, HF-C: Hevelius Formation continuous facies, and HF-DC: Hevelius Formation discontinuous facies. The points in DF represent 35 spectra extraction outcrops in the SPA outer ring (purple), Das crater region (dark cyan), and Sternfeld crater region (green).

large distance. In the eastern portion of the Sternfeld-Das region, the Hertzsprung basin ejecta from the north and the Hevelius Formation from the east contact, with the latter (Hevelius) superposed on the up layer (Figure 4c). The Hevelius Formation shows pronounced radial texture and buries all of the substrata in the continuous facies, but it decays to become thinner and discontinuous in the Sternfeld-Das region. In the geologic map of the northern portion of the SPA basin completed by Ivanov et al. (2018), the Sternfeld-Das region is mapped as SPA rim material, which represents the ejecta from the SPA impact.

To obtain the mineralogic properties of the Sternfeld-Das region, we identified 35 outcrops where the surface matured regolith has been removed by fresh impacts and then performed the spectroscopic analysis of the exposed material using Moon Mineralogy Mapper (M^3) data (Green et al., 2011). For each outcrop, the spectrum is an averaged product of multiple pixels with absorption features to decrease the noise. In the 35 outcrops, 33 are young craters with diameters less than 2 km and 2 are from the wall of the 36 km-diameter Das crater. Though the outcrop craters are small in size, the predominate regolith component of the investigation area is SPA ejecta (discussed in section 4.1). Moreover, many of these outcrops are located on the wall or rim of much larger craters, where the substrata can be directly observed, such as the Das crater. We divided the outcrops into three groups for comparative analysis, which are the SPA outer ring, the Sternfeld region, and the Das region (Figures 4c and S2). The SPA outer ring (i.e., the SPA rim) provides the most trustworthy representation of the SPA ejecta, while the Sternfeld region and Das region are mostly affected by two different sources of modification, the Korolev basin and the Orientale basin, respectively. Using the method of Horgan et al. (2014), we calculated the absorption parameters of the spectra as shown in Figure 5, which also shows the parameters of natural and synthetic OPX and clinopyroxene

(CPX) for comparison. The results suggest that the spectral absorptions of the three groups are indistinguishable and they are consistent with the OPX-bearing materials interpreted to be from the mantle (Figure 5a) (Melosh et al., 2017). Relatively higher Fe abundance in the investigation area than the highland terrain was also revealed by Moriarty and Pieters (2018). The band parameter space of different minerals and mixing trends suggest that the material may be mixed with olivine from the mantle and impact glass (Figure 5b). The geological context and compositional characteristics of outcrops collectively demonstrate that the Sternfeld-Das region is the rock-stratigraphic unit composed of the SPA ejecta. One notable site is the Das crater, which was formed during the Copernican Period as evidenced by its optical maturity (Figure 6b). With an average rim-to-floor depth of ~3.5 km (Figure S3), the crater wall serves as a representative exposure of the SPA ejecta deposit stratum. An outcrop spectrum of the wall is shown in Figure 6c, where the band centers indicate that OPX is the dominate silicate mineral. The additional absorption at ~1.2–1.3 μm suggests that the material may have a significant portion of plagioclase or impact glasses and other minerals (Horgan et al., 2014). Due to the significance of Das crater to the understanding of the SPA ejecta deposit, we designate this exposed rock-stratigraphic unit in the Sternfeld-Das region as Das Formation (Figure 4c), which represents the stratum formed by the ejecta from the SPA cratering process. In the time scale scheme of the Moon, the Das Formation is equivalent to the "golden spike" of the chronostratigraphic scale of the Earth (Gradstein and Ogg, 2020).

4.2.2 *The geological cross-section and stratotype*

To illustrate the regional geology and evolutionary history, we created a schematic geological cross-section (Figure 7b) along P1-P2-P3 shown in Figures 4a and 7a. The oldest stratum is the primary crust crystallized in Magma-oceanian Period and underlies the Das Formation (Petro and Pieters, 2008). The SPA ejecta deposit, i.e., the Das Formation, is the lower boundary of the Aitkenian Period. The ejecta of subsequent Nectarian basins, including Korolev and Hertzsprung, overlapped large areas of the Das Formation, and are in turn overlain by the Imbrian-aged spatially heterogeneous Hevelius Formation. The interior material of the Orientale basin, named Montes Rook Formation (Scott and McCauley, 1977), might represent the ejecta facies derived from a depth greater than the material of Hevelius Formation (Head, 1974). Ejecta from large craters and basins at greater distances could also transport materials to this region but were of insufficient thickness to form recognizable rock-stratigraphic units. Small craters (i.e., Mechnikov, Sternfeld, Das, and Ellerman) on the cross-section gardened local regolith, forming mixtures between different strata. With relatively sharp rim structure and terraces (Figure 6a), the Copernican-aged Das crater exposes the immature Das Formation in its collapsed fresh wall.

5. The stratigraphic column of the Moon

The lunar stratigraphic column synthesized by Wilhelms et al. (1987) shows the major rock-stratigraphic units corresponding to the five time scale Periods. The pre-Nectarian Period includes three groups of rock-stratigraphic units: these have been interpreted to have formed predominantly as early crustal rocks, volcanic materials, and basin and crater materials. In our updated time scale, the early crustal rocks, which were mainly generated from the solidification of the magma ocean, belong to the Magma-oceanian Period,

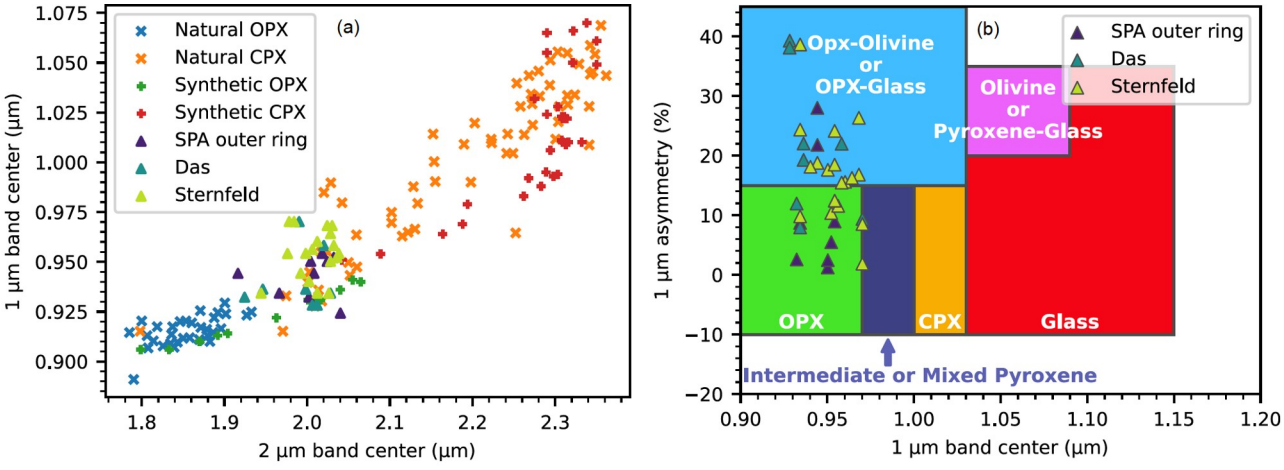

Figure 5 (a) The band centers at 1 and 2 μm of the 35 outcrop spectra extracted from the SPA outer ring, Das crater region, and Sternfeld crater region. Natural and synthetic pure CPX and OPX are provided for comparison (Cloutis and Gaffey, 1991; Klima et al., 2011). (b) Band parameter space of different minerals and mixing trends of the Moon as defined by Horgan et al. (2014). The band asymmetry is defined as the difference of the left and right absorption areas, as a percent of the total area (Horgan et al., 2014).

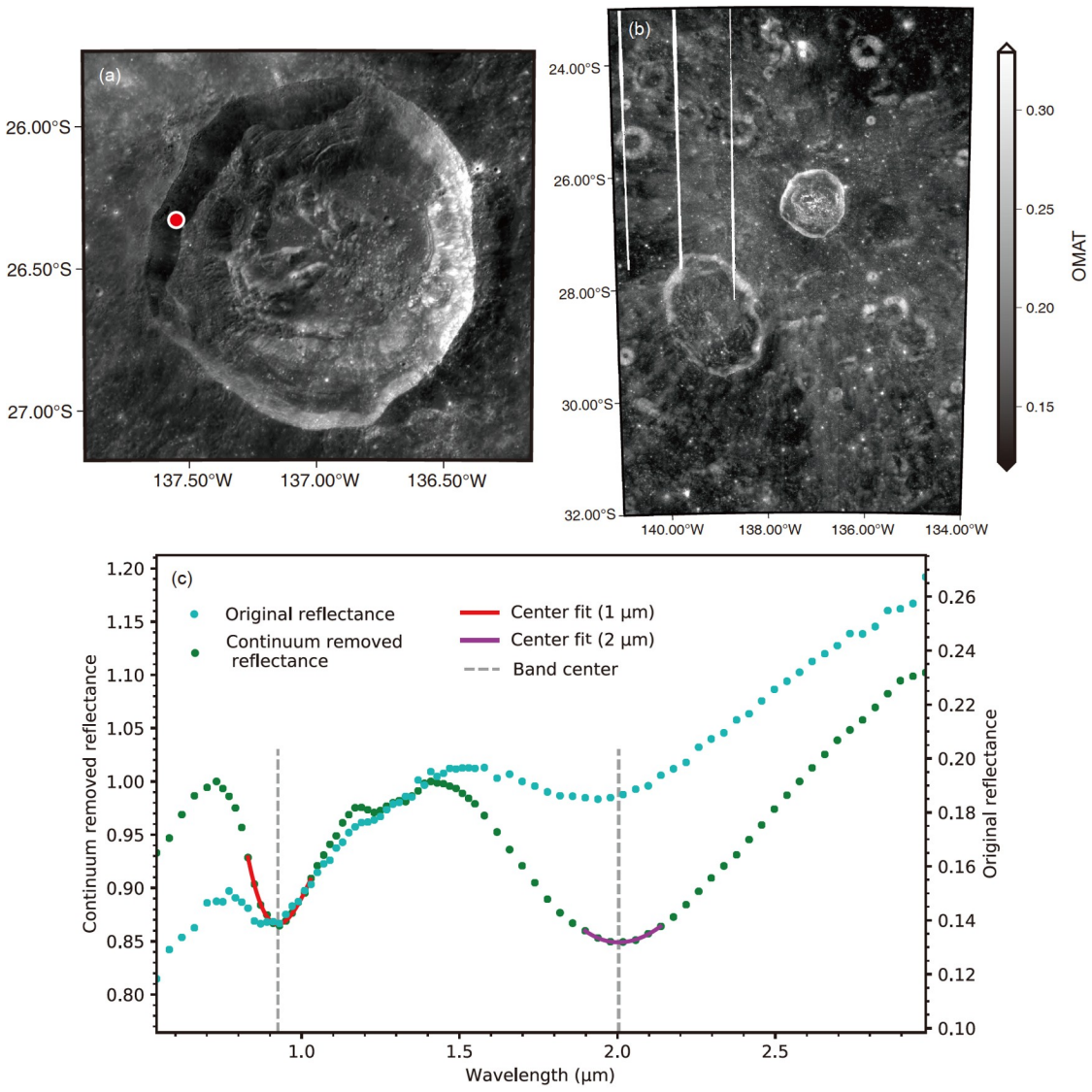

Figure 6 (a) The Das crater (36 km in diameter) shown on the Chang'e-2 CCD images (7 m pixel^{-1}). The red point on the crater wall designates the location where the spectrum displayed in (c) was obtained. (b) Optical maturity (OMAT) of the Das crater region, where the ray system in bright tune indicates a Copernican-aged crater. The three white strips on the left side are a result of missing data. (c) The spectrum and process results of Das crater wall. The method of Horgan et al. (2014) was utilized for continuum-removing and band center fits processing. The absorption centers of 1 μm band and 2 μm band are 0.92 μm and 2.01 μm, respectively.

while the other two groups of materials belong to the Aitkenian Period, subsequent to a rigid primordial crust was formed. This updated stratigraphic column is shown in Figure 8, and consists of two major changes. First, the three Eonothem units provide the highest level of the stratigraphic system. Second, the rock-stratigraphic units of the pre-Nectarian are separated into Magma-oceanian System and Aitkenian System. The Das Formation, which represents materials of the ejecta deposit of the SPA basin, is the lowest stratum of the Aitkenian System, overlain by postdated basin ejecta and probably with intrusive rocks. The other Periods remain the same as defined by Wilhelms et al. (1987). The Nectaris basin, ~3.92 Ga in age, marks the beginning of the Nectarian Period, during which ejecta deposits of large basins and magmatism products compose the major strata. The Lower Imbrian Epoch materials are bounded by the Imbrium ejecta (Fra Mauro Formation) and Orientale ejecta (Hevelius Formation) at the bottom and top, respectively. In the Upper Imbrian Epoch, volcanic materials (i.e., mare basalts), flooded the floors and interior of preexisting craters and basins and are the major components of this Epoch. Subsequently, endogenic heat production and processes attenuated and large-scale volcanic activity significantly waned, especially in the Copernican Period. During the Eratosthenian and Copernican Periods, the major materials emplaced on lunar surface are ejecta of young craters and the Copernican craters, younger in age, show prominent ejecta ray systems.

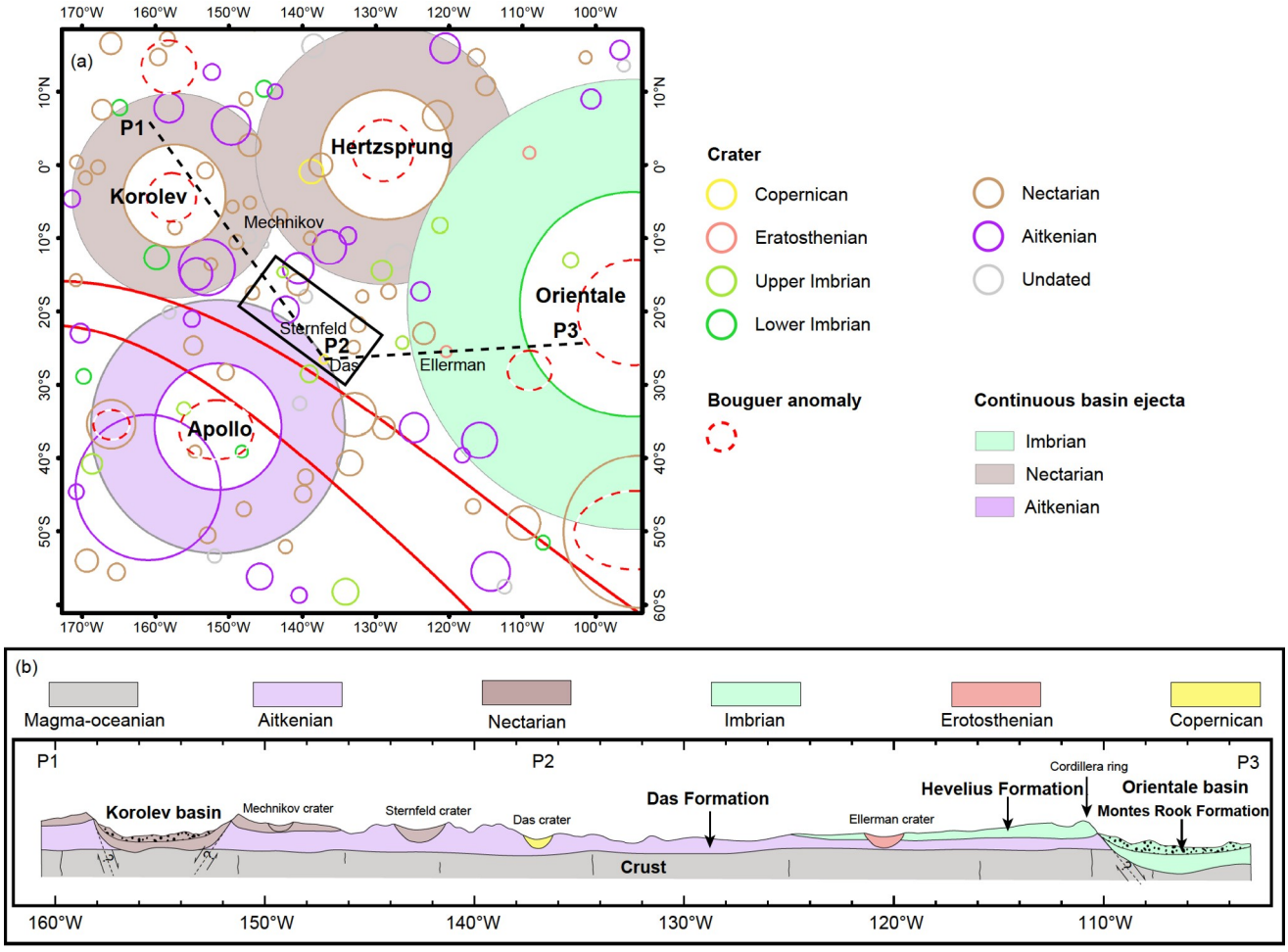

Figure 7 (a) Schematic map of the northeastern SPA region. The map shows craters with diameters larger than 50 km and two smaller craters situated on the cross-section trace, Das crater (36 km) and Ellerman crater (46 km). The shadowed region represents the annulus of 1–2 radii from the parent crater center, where the continuous ejecta facies distribute. The red solid lines represent the SPA inner ring and outer ring. The black square shows the location of the Sternfeld-Das region where the spectroscopic features suggest that the materials are dominated by the SPA ejecta deposit. The Bouguer gravity anomaly is based on Neumann et al. (2015). The black dashed line P1-P2-P3 denotes the trace of the schematic geologic cross-section of (b).

6. Discussion and outlook

The geologic time scale is of fundamental importance in planetary geological studies and geological mapping. The current lunar time scale documented and synthesized by Wilhelms et al. (1987) was created from regional geologic mappings in the Apollo era, primarily of the nearside of the Moon. Subsequently, and in the study of the petrologic and geophysical evolution of the Moon (Jolliff et al., 2006), much more considerations have been given to global-scale lunar evolution, including the geology of the farside, where the SPA basin formed and significantly influenced the global evolution of the Moon (Petro and Pieters, 2008; Schultz et al., 2011; Melosh et al., 2017; Jones et al., 2022; Zhang et al., 2022). Our updates to the lunar time scale clearly show the more synergistic three-phase dynamical evolution of the Moon, while introducing minimal changes to the time scale presently in use. The SPA basin, as the oldest recognizable impact basin (Orgel et al., 2018), marks a key transition in lunar evolution history. Separating the basin formation events during the pre-Nectarian of Wilhelms et al. (1987) is important in studying the beginning and early stages of large impact processes on the Moon. During the Aitkenian, the thermal gradient was steeper than in later Periods, resulting in important differences in basin formation and relaxation processes (Miljković et al., 2013, 2021; Zhu et al., 2017). The other important modification to the Wilhelms et al. (1987) framework is that magma ocean dominated evolution is defined as an individual Period (Table 1; Figure 8), making it a more convenient factor in studying primordial crustal materials of the initial Moon and early lunar history. In our time scale, the six Period/System-level units are allocated to three Eon/Eonothem-level units based on the dynamical themes (Table 1; Figure 8). This treatment provides a framework to view the evolution of the Moon from a more comprehensive and synergistic perspective.

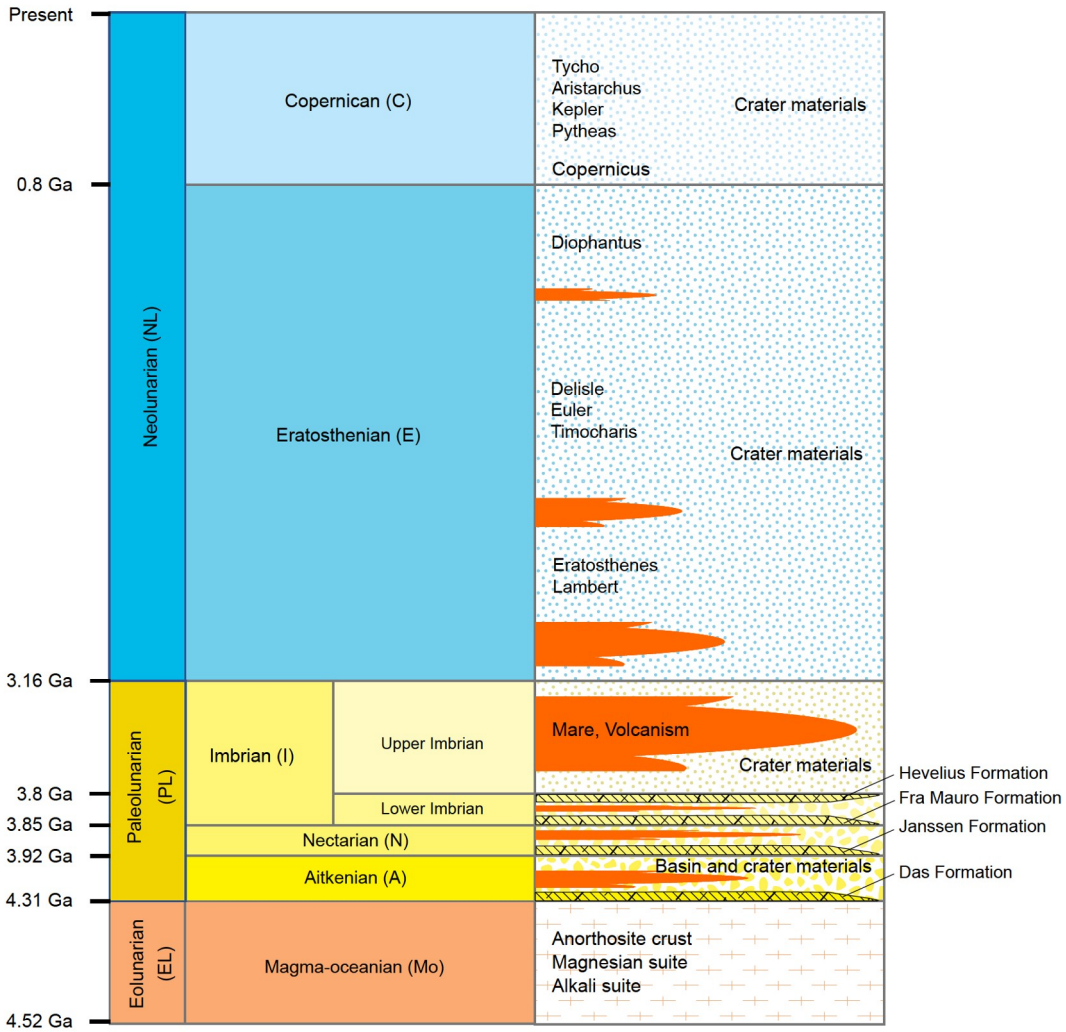

Figure 8 The stratigraphic column of the Moon that is modified from Wilhelms et al. (1987) according to the updated time scale system described in this study. Note that the heights of the units are not accurately scaled to the time range. The red bar in the stratigraphic column indicates mare eruption and volcanism.

Our suggested modifications to the current lunar time scale are designed to provide an updated perspective on the history and dynamic evolution of the Moon. There remain several additional unsolved concerns that should be addressed in the future. The uncertainty of absolute ages of the time scale units, which has been widely discussed in many literatures (e.g., Stöffler and Ryder, 2001; Hiesinger and Tanaka, 2020), is one of the most important issues to be resolved. As for the Aitkenian Period, samples returned from the SPA basin and South Pole region will provide determined constraints. The Lower Imbrian and Upper Imbrian, as two subunits of the Imbrian Period, were initially interpreted to distinguish highlands materials and mare basalts, respectively (Wilhelms, 1970). The dividing event was defined at the Orientale impact basin, because in part it appeared to be older than the maria (since shown by the presence of cryptomaria to be incorrect (Whitten and Head, 2015)), and younger than the Imbrium basin judging from its well-preserved morphology (Wilhelms et al., 1987). However, as the youngest megabasin, the Orientale impact basin can play an additional important role in the lunar time scale system. The Neolunarian Eonothem includes two Systems, i.e., Eratosthenian and Copernican (Table 1). These were defined in the initial time scale of Shoemaker and Hackman (1962) to describe the post-mare crater materials, and the Eratosthenian System did not initially contain mare material. The stratigraphic basis of the Eratosthenian System was not well defined (being distinguished from the Copernican by the absence of bright rays) and the geological units were assigned to this System by quantitative thresholds on crater erosion status and crater frequencies (Wilhelms et al., 1987). Maria eruptions in the early Eratosthenian are much more extensive than the late Eratosthenian (Hiesinger et al., 2011; Morota et al., 2011), a pattern suggesting that Eratosthenian volcanic activity is a continuation of Imbrian volcanism. The dividing at 3.16 Ga was based on the relative young mare plain of the Apollo 12

sampling region and did not take into consideration of the whole-Moon endogenic evolution (Shoemaker and Hackman, 1962). However, samples returned from the Chang'e-5 mission have proved that lunar volcanism lasted to at least ~2.0 Ga (Che et al., 2021; Li et al., 2021), and evidence for possible Copernican-aged volcanic activity has recently been proposed (Braden et al., 2014), but is debated (Qiao et al., 2017). Moreover, the Eratosthenian Period has an extremely long time range of more than half of lunar history (Wilhelms et al., 1987). Thus, more efforts should be paid to dating craters and mare materials, and potentially subdividing this Period at the last mare eruption that resurfaced the Moon at substantial scale. The stratigraphic basis of the Copernican System was neither initially defined in detail. Copernican craters are characterized by prominent ray systems, but many craters with this feature are consist of compositional rays, not degradational processes (Hawke et al., 2004), and many are also older than Copernicus crater (Wilhelms et al., 1987; Hiesinger and Tanaka, 2020). Due to these uncertainties in the stratigraphic basis for the Eratosthenian and Copernican, the absolute ages for their boundaries are uncertain and debated (Stöffler and Ryder, 2001). To further improve the time scale and make it consummate and more cogent, it is important to allocate additional efforts on these matters during future research and landing and sample-return missions, especially to the farside and polar regions.

In the latest 1:2,500,000-scale geologic map of the global Moon (Ji et al., 2022), this updated time scale was applied, providing a good framework to understand the global-scale geologic map. Because the magma ocean, intensive bombardments, and volcanism are generally thought as common processes in terrestrial planets such as Mercury and Mars (Bottke and Norman, 2017; Elkins-Tanton, 2012), the lunar time scale based on its dynamical evolution may serve to assist communication not only in the study of the Moon but also in comparative planetology of the terrestrial planets.

7. Conclusions

We carried out a comprehensive overview and analysis of lunar geologic evolution with respect to the nature and relationship of dynamical changes, i.e., endogenic and exogenic evolution. The temporal interplay of exogenic and endogenic processes in altering the Moon indicates that the evolution history of the Moon can be divided into three dynamic evolutionary phases. From a geochronologic perspective, the three phases are designated as three Eon/Eonothem-level units, which are Eolunarian, Paleolunarian, and Neolunarian from old to young. The pre-Necterian Period in the current time scale is divided into Magma-oceanian Period and Aitkenian Period, with the rock-stratigraphic boundary defined at the Das Formation, the stratum formed by the SPA ejecta deposit. The Eolunarian lasts from the formation of the Moon to the solidification of the magma ocean and is endogenic-dominated. The Paleolunarian is characterized by both active endogenic and exogenic processes. Beginning with the SPA basin, the Paleolunarian includes three Period-level units: Aitkenian, Nectarian, and Imbrian. The Neolunarian Eon includes two Periods (i.e., Eratosthenian and Copernican) and exogenic processes (i.e., meteorite impacts) are the controlling factors in modifying lunar surface. The updated lunar time scale paradigm provides a basic framework to illustrate the evolution history of the Moon and can be applied in lunar geological study and geological mapping work. In future explorations, it is significant to return samples from the unsampled farside and polar regions to complete the lunar time scale and improve our understanding of the evolution of the Moon.

Acknowledgements *We thank Briony H.N. HORGAN for the discussion on M^3 data processing. We are grateful for the teams working for LROC, LOLA and M^3 data, which can be obtained at NASA's Planetary Data System (http://pds.nasa.gov/). The Chinese Lunar Exploration Program and the exploration data are available at Lunar and Deep Space Exploration Scientific Data and Sample Release System (http://202.106.152.98:8081/moondata/). The data used for calculation and figure plotting can be downloaded at http://doi.org/10.12176/03.99.02174. This work was supported partly by the National Key Research and Development Program of China (Grant No. 2022YFF0503100), the B-type Strategic Priority Program of the Chinese Academy of Sciences (Grant No. XDB41000000), the National Natural Science Foundation of China (Grant Nos. 41902317, 41941002, 41773065), and the National Science and Technology Infrastructure Work Projects (Grant No. 2015FY210500).*

Conflict of interest The authors declare that they have no conflict of interest.

References

Baker D M H, Head J W, Phillips R J, Neumann G A, Bierson C J, Smith D E, Zuber M T. 2017. GRAIL gravity observations of the transition from complex crater to peak-ring basin on the Moon: Implications for crustal structure and impact basin formation. Icarus, 292: 54–73

Barr A C. 2016. On the origin of Earth's Moon. J Geophys Res-Planets, 121: 1573–1601

Boehnke P, Harrison T M. 2016. Illusory late heavy bombardments. Proc Natl Acad Sci USA, 113: 10802–10806

Borg L E, Gaffney A M, Shearer C K. 2015. A review of lunar chronology revealing a preponderance of 4.34-4.37 Ga ages. Meteorit Planet Sci, 50: 715–732

Borg L, Norman M, Nyquist L, Bogard D, Snyder G, Taylor L, Lindstrom M. 1999. Isotopic studies of ferroan anorthosite 62236: A young lunar crustal rock from a light rare-earth-element-depleted source. Geochim Cosmochim Acta, 63: 2679–2691

Bottke W F, Norman M D. 2017. The late heavy bombardment. Annu Rev Earth Planet Sci, 45: 619–647

Boyet M, Carlson R W, Borg L E, Horan M. 2015. Sm-Nd systematics of lunar ferroan anorthositic suite rocks: Constraints on lunar crust formation. Geochim Cosmochim Acta, 148: 203–218

Braden S E, Stopar J D, Robinson M S, Lawrence S J, van der Bogert C H, Hiesinger H. 2014. Evidence for basaltic volcanism on the Moon within the past 100 million years. Nat Geosci, 7: 787–791

Canup R M. 2012. Forming a moon with an Earth-like composition via a giant impact. Science, 338: 1052–1055
Che X, Nemchin A, Liu D, Long T, Wang C, Norman M D, Joy K H, Tartese R, Head J, Jolliff B, Snape J F, Neal C R, Whitehouse M J, Crow C, Benedix G, Jourdan F, Yang Z, Yang C, Liu J, Xie S, Bao Z, Fan R, Li D, Li Z, Webb S G. 2021. Age and composition of young basalts on the Moon, measured from samples returned by Chang'e-5. Science, 374: 887–890
Cloutis E A, Gaffey M J. 1991. Pyroxene spectroscopy revisited: Spectral-compositional correlations and relationship to geothermometry. J Geophys Res, 96: 22809–22826
Cohen K M, Finney S C, Gibbard P L, Fan J X. 2013. The ICS international chronostratigraphic chart. Episodes, 36: 199–204
Collins G S, Melosh H J, Osinski G R. 2012. The impact-cratering process. Elements, 8: 25–30
Collins G S, Patel N, Davison T M, Rae A S P, Morgan J V, Gulick S P S, Christeson G L, Chenot E, Claeys P, Cockell C S, Coolen M J L, Ferrière L, Gebhardt C, Goto K, Jones H, Kring D A, Lofi J, Lowery C M, Ocampo-Torres R, Perez-Cruz L, Pickersgill A E, Poelchau M H, Rasmussen C, Rebolledo-Vieyra M, Riller U, Sato H, Smit J, Tikoo S M, Tomioka N, Urrutia-Fucugauchi J, Whalen M T, Wittmann A, Xiao L, Yamaguchi K E, Artemieva N, Bralower T J. 2020. A steeply-inclined trajectory for the Chicxulub impact. Nat Commun, 11: 1480
Conrad J W, Nimmo F, Fassett C I, Kamata S. 2018. Lunar impact history constrained by GRAIL-derived basin relaxation measurements. Icarus, 314: 50–63
Curran N M, Joy K H, Snape J F, Pernet-Fisher J F, Gilmour J D, Nemchin A A, Whitehouse M J, Burgess R. 2019. The early geological history of the Moon inferred from ancient lunar meteorite Miller Range 13317. Meteorit Planet Scien, 54: 1401–1430
Elkins-Tanton L T, Burgess S, Yin Q Z. 2011. The lunar magma ocean: Reconciling the solidification process with lunar petrology and geochronology. Earth Planet Sci Lett, 304: 326–336
Elkins-Tanton L T. 2012. Magma oceans in the inner solar system. Annu Rev Earth Planet Sci, 40: 113–139
Fischer-Gödde M, Becker H. 2011. What is the age of the Nectaris basin? New Re-Os constraints for a pre-4.0 Ga bombardment history of the Moon. Lunar and Planetary Sciecne Conference. 1414
Garrick-Bethell I, Miljković K, Hiesinger H, van der Bogert C H, Laneuville M, Shuster D L, Korycansky D G. 2020. Troctolite 76535: A sample of the Moon's South Pole-Aitken basin? Icarus, 338: 113430
Garrick-Bethell I, Zuber M T. 2009. Elliptical structure of the lunar South Pole-Aitken basin. Icarus, 204: 399–408
Gomes R, Levison H F, Tsiganis K, Morbidelli A. 2005. Origin of the cataclysmic Late Heavy Bombardment period of the terrestrial planets. Nature, 435: 466–469
Gradstein F M, Ogg J G, Schmitz M D, Ogg G M. 2020. Geologic Time Scale 2020. Amsterdam, Netherlands: Elsevier
Gradstein F M, Ogg J G. 2020. Chapter 2—The Chronostratigraphic Scale. In: Gradstein F M, Ogg J G, Schmitz M D, Ogg G M, eds. Geologic Time Scale 2020. Amsterdam: Elsevier. 21–32
Green R O, Pieters C, Mouroulis P, Eastwood M, Boardman J, Glavich T, Isaacson P, Annadurai M, Besse S, Barr D, Buratti B, Cate D, Chatterjee A, Clark R, Cheek L, Combe J, Dhingra D, Essandoh V, Geier S, Goswami J N, Green R, Haemmerle V, Head J, Hovland L, Hyman S, Klima R, Koch T, Kramer G, Kumar A S K, Lee K, Lundeen S, Malaret E, McCord T, McLaughlin S, Mustard J, Nettles J, Petro N, Plourde K, Racho C, Rodriquez J, Runyon C, Sellar G, Smith C, Sobel H, Staid M, Sunshine J, Taylor L, Thaisen K, Tompkins S, Tseng H, Vane G, Varanasi P, White M, Wilson D. 2011. The Moon Mineralogy Mapper (M^3) imaging spectrometer for lunar science: Instrument description, calibration, on-orbit measurements, science data calibration and on-orbit validation. J Geophys Res, 116: e00G19
Gross J, Joy K H. 2016. Evolution, lunar: From magma ocean to crust formation. In: Cudnik B, ed. Encyclopedia of Lunar Science. Cham, Switzerland: Springer International Publishing
Gustafson J O, Bell J F, Gaddis L R, Hawke B R, Giguere T A. 2012. Characterization of previously unidentified lunar pyroclastic deposits using Lunar Reconnaissance Orbiter Camera data. J Geophys Res, 117: e00H25
Hawke B R, Blewett D T, Lucey P G, Smith G A, Bell Iii J F, Campbell B A, Robinson M S. 2004. The origin of lunar crater rays. Icarus, 170: 1–16
Head J W, Fassett C I, Kadish S J, Smith D E, Zuber M T, Neumann G A, Mazarico E. 2010. Global distribution of large lunar Craters: Implications for resurfacing and impactor populations. Science, 329: 1504–1507
Head J W, Pieters C, McCord T, Adams J, Zisk S. 1978. Definition and detailed characterization of lunar surface units using remote observations. Icarus, 33: 145–172
Head J W, Wilson L. 1992. Lunar mare volcanism: Stratigraphy, eruption conditions, and the evolution of secondary crusts. Geochim Cosmochim Acta, 56: 2155–2175
Head J W, Wilson L. 2017. Generation, ascent and eruption of magma on the Moon: New insights into source depths, magma supply, intrusions and effusive/explosive eruptions (Part 2: Predicted emplacement processes and observations). Icarus, 283: 176–223
Head J W. 1974. Orientale multi-ringed basin interior and implications for the petrogenesis of lunar highland samples. Moon, 11: 327–356
Hess P C, Parmentier E M. 1995. A model for the thermal and chemical evolution of the Moon's interior: Implications for the onset of mare volcanism. Earth Planet Sci Lett, 134: 501–514
Hiesinger H, Head III J W, Wolf U, Jaumann R, Neukum G, Ambrose W A, Williams D A. 2011. Ages and stratigraphy of lunar mare basalts: A synthesis. In: Ambrose W A, Williams D A, eds. Recent Advances and Current Research Issues in Lunar Stratigraphy. Geological Society of America. 1–51
Hiesinger H, Head J W, Wolf U, Jaumann R, Neukum G. 2010. Ages and stratigraphy of lunar mare basalts in Mare Frigoris and other nearside maria based on crater size-frequency distribution measurements. J Geophys Res, 115: e03003
Hiesinger H, Tanaka K. 2020. Chapter 15—The Planetary Time Scale. In: Gradstein F M, Ogg J G, Schmitz M D, Ogg G M, eds. Geologic Time Scale 2020. Amsterdam, Netherlands: Elsevier. 443–480
Hiesinger H, van der Bogert C, Pasckert J, Schmedemann N, Robinson M, Jolliff B, Petro N. 2012. New crater size-frequency distribution measurements of the South Pole-Aitken basin. In: 43rd Lunar and Planetary Science Conference. 43: 2863
Holsapple K A. 1993. The scaling of impact processes in planetary sciences. Annu Rev Earth Planet Sci, 21: 333–373
Horgan B H N, Cloutis E A, Mann P, Bell J F. 2014. Near-infrared spectra of ferrous mineral mixtures and methods for their identification in planetary surface spectra. Icarus, 234: 132–154
Hörz F, Brownlee D E, Fechtig H, Hartung J B, Morrison D A, Neukum G, Schneider E, Vedder J F, Gault D E. 1975. Lunar microcraters: Implications for the micrometeoroid complex. Planet Space Sci, 23: 151–172
Housen K R, Schmidt R M, Holsapple K A. 1983. Crater ejecta scaling laws: Fundamental forms based on dimensional analysis. J Geophys Res, 88: 2485–2499
Huang Y H, Soderblom J M, Minton D A, Hirabayashi M, Melosh H J. 2022. Bombardment history of the Moon constrained by crustal porosity. Nat Geosci, 15: 531–535
Ivanov M A, Hiesinger H, van der Bogert C H, Orgel C, Pasckert J H, Head J W. 2018. Geologic history of the northern portion of the South Pole-Aitken basin on the Moon. J Geophys Res-Planets, 123: 2585–2612
Ji J, Guo D, Liu J, Chen S, Ling Z, Ding X, Han K, Chen J, Cheng W, Zhu K, Liu J, Wang J, Chen J, Ouyang Z. 2022. The 1:2,500,000-scale geologic map of the global Moon. Sci Bull, 67: 1544–1548
Johnson B C, Blair D M, Collins G S, Melosh H J, Freed A M, Taylor G J, Head J W, Wieczorek M A, Andrews-Hanna J C, Nimmo F, Keane J T, Miljkovi K, Soderblom J M, Zuber M T. 2016. Formation of the Orientale lunar multiring basin. Science, 354: 441–444
Jolliff B L, Gillis J J, Haskin L A, Korotev R L, Wieczorek M A. 2000.

Major lunar crustal terranes: Surface expressions and crust-mantle origins. J Geophys Res, 105: 4197–4216
Jolliff B L, Wieczorek M A, Shearer C K, Neal C R. 2006. New views of the Moon. Chantilly, Virginia: Mineralogical Society of America
Jones M J, Evans A J, Johnson B C, Weller M B, Andrews-Hanna J C, Tikoo S M, Keane J T. 2022. A South Pole-Aitken impact origin of the lunar compositional asymmetry. Sci Adv, 8: eabm8475
Klima R L, Pieters C M, Boardman J W, Green R O, Head Iii J W, Isaacson P J, Mustard J F, Nettles J W, Petro N E, Staid M I, Sunshine J M, Taylor L A, Tompkins S. 2011. New insights into lunar petrology: Distribution and composition of prominent low-Ca pyroxene exposures as observed by the Moon Mineralogy Mapper (M^3). J Geophys Res, 116: e00G06
Laneuville M, Taylor J, Wieczorek M A. 2018. Distribution of radioactive heat sources and thermal history of the Moon. J Geophys Res-Planets, 123: 3144–3166
Laneuville M, Wieczorek M A, Breuer D, Tosi N. 2013. Asymmetric thermal evolution of the Moon. J Geophys Res-Planets, 118: 1435–1452
Le Feuvre M, Wieczorek M A. 2008. Nonuniform cratering of the terrestrial planets. Icarus, 197: 291–306
Lee D C, Halliday A N, Snyder G A, Taylor L A. 1997. Age and origin of the Moon. Science, 278: 1098–1103
Li C, Hu H, Yang M F, Pei Z Y, Zhou Q, Ren X, Liu B, Liu D, Zeng X, Zhang G, Zhang H, Liu J, Wang Q, Deng X, Xiao C, Yao Y, Xue D, Zuo W, Su Y, Wen W, Ouyang Z. 2022. Characteristics of the lunar samples returned by the Chang'E-5 mission. Natl Sci Rev, 9: Nwab188
Li Q L, Zhou Q, Liu Y, Xiao Z, Lin Y, Li J H, Ma H X, Tang G Q, Guo S, Tang X, Yuan J Y, Li J, Wu F Y, Ouyang Z, Li C, Li X H. 2021. Two-billion-year-old volcanism on the Moon from Chang'e-5 basalts. Nature, 600: 54–58
Liu J, Liu J, Yue Z, Zhang L, Wang J, Zhu K. 2022. Characterization and interpretation of the global lunar impact basins based on remote sensing. Icarus, 378: 114952
Lock S J, Stewart S T, Petaev M I, Leinhardt Z, Mace M T, Jacobsen S B, Cuk M. 2018. The origin of the Moon within a terrestrial synestia. J Geophys Res-Planets, 123: 910–951
Marks N E, Borg L E, Shearer C K, Cassata W S. 2019. Geochronology of an Apollo 16 clast provides evidence for a basin-forming impact 4.3 billion years ago. J Geophys Res-Planets, 124: 2465–2481
Maurice M, Tosi N, Schwinger S, Breuer D, Kleine T. 2020. A long-lived magma ocean on a young Moon. Sci Adv, 6: eaba8949
Mazrouei S, Ghent R R, Bottke W F, Parker A H, Gernon T M. 2019. Earth and Moon impact flux increased at the end of the Paleozoic. Science, 363: 253–257
McCauley J F. 1966. The nature of the lunar surface as determined by systematic geologic mapping. Mant Earth Terrestr Planet, 1: 431–460
Melosh H J, Kendall J, Horgan B, Johnson B C, Bowling T, Lucey P G, Taylor G J. 2017. South Pole-Aitken basin ejecta reveal the Moon's upper mantle. Geology, 45: 1063–1066
Mighani S, Wang H, Shuster D L, Borlina C S, Nichols C I O, Weiss B P. 2020. The end of the lunar dynamo. Sci Adv, 6: eaax0883
Miljković K, Wieczorek M A, Collins G S, Laneuville M, Neumann G A, Melosh H J, Solomon S C, Phillips R J, Smith D E, Zuber M T. 2013. Asymmetric distribution of lunar impact basins caused by variations in target properties. Science, 342: 724–726
Miljković K, Wieczorek M A, Laneuville M, Nemchin A, Bland P A, Zuber M T. 2021. Large impact cratering during lunar magma ocean solidification. Nat Commun, 12: 5433
Morbidelli A, Nesvorny D, Laurenz V, Marchi S, Rubie D C, Elkins-Tanton L, Wieczorek M, Jacobson S. 2018. The timeline of the lunar bombardment: Revisited. Icarus, 305: 262–276
Moriarty D P, Pieters C M. 2018. The character of South Pole-Aitken basin: Patterns of surface and sub-surface composition. J Geophys Res-Planets, 123: 729–747
Morota T, Haruyama J, Ohtake M, Matsunaga T, Honda C, Yokota Y, Kimura J, Ogawa Y, Hirata N, Demura H, Iwasaki A, Sugihara T, Saiki K, Nakamura R, Kobayashi S, Ishihara Y, Takeda H, Hiesinger H. 2011. Timing and characteristics of the latest mare eruption on the Moon. Earth Planet Sci Lett, 302: 255–266
Neal C R, Taylor L A. 1992. Petrogenesis of mare basalts: A record of lunar volcanism. Geochim Cosmochim Acta, 56: 2177–2211
Nemchin A A, Long T, Jolliff B L, Wan Y, Snape J F, Zeigler R, Grange M L, Liu D, Whitehouse M J, Timms N E, Jourdan F. 2021. Ages of lunar impact breccias: Limits for timing of the Imbrium impact. Geochemistry, 81: 125683
Nesvorný D, Roig F. 2018. Dynamical origin and terrestrial impact flux of large near-Earth asteroids. Astron J, 155: 42
Neukum G, Ivanov B A, Hartmann W K. 2001. Cratering records in the inner solar system in relation to the lunar reference system. Space Sci Rev, 96: 55–86
Neukum G, Ivanov B A. 1994. Crater size distributions and impact probabilities on Earth from lunar, terrestrial-planet, and asteroid cratering data. In: Gehrels T G, ed. Hazards due to Comets and Asteroids. Tucson: University of Arizona Press. 359–416
Neumann G A, Zuber M T, Wieczorek M A, Head J W, Baker D M H, Solomon S C, Smith D E, Lemoine F G, Mazarico E, Sabaka T J, Goossens S J, Melosh H J, Phillips R J, Asmar S W, Konopliv A S, Williams J G, Sori M M, Soderblom J M, Miljković K, Andrews-Hanna J C, Nimmo F, Kiefer W S. 2015. Lunar impact basins revealed by Gravity Recovery and Interior Laboratory measurements. Sci Adv, 1: e1500852
Norman M D, Duncan R A, Huard J J. 2010. Imbrium provenance for the Apollo 16 Descartes terrain: Argon ages and geochemistry of lunar breccias 67016 and 67455. Geochim Cosmochim Acta, 74: 763–783
Norman M D, Nemchin A A. 2014. A 4.2 billion year old impact basin on the Moon: U-Pb dating of zirconolite and apatite in lunar melt rock 67955. Earth Planet Sci Lett, 388: 387–398
Nyquist L E, Shih C Y. 1992. The isotopic record of lunar volcanism. Geochim Cosmochim Acta, 56: 2213–2234
Ohtake M, Matsunaga T, Haruyama J, Yokota Y, Morota T, Honda C, Ogawa Y, Torii M, Miyamoto H, Arai T, Hirata N, Iwasaki A, Nakamura R, Hiroi T, Sugihara T, Takeda H, Otake H, Pieters C M, Saiki K, Kitazato K, Abe M, Asada N, Demura H, Yamaguchi Y, Sasaki S, Kodama S, Terazono J, Shirao M, Yamaji A, Minami S, Akiyama H, Josset J L. 2009. The global distribution of pure anorthosite on the Moon. Nature, 461: 236–240
Orgel C, Michael G, Fassett C I, van der Bogert C H, Riedel C, Kneissl T, Hiesinger H. 2018. Ancient bombardment of the inner solar system: Reinvestigation of the "fingerprints" of different impactor populations on the lunar surface. J Geophys Res-Planets, 123: 748–762
Perera V, Jackson Alan P, Elkins-Tanton Linda T, Asphaug E. 2018. Effect of reimpacting debris on the solidification of the lunar Magma Ocean. J Geophys Res-Planets, 123: 1168–1191
Petro N E, Pieters C M. 2006. Modeling the provenance of the Apollo 16 regolith. J Geophys Res, 111: e09005
Petro N E, Pieters C M. 2008. The lunar-wide effects of basin ejecta distribution on the early megaregolith. Meteorit Planet Sci, 43: 1517–1529
Pike R J. 1974. Ejecta from large craters on the Moon: Comments on the geometric model of McGetchin et al.. Earth Planet Sci Lett, 23: 265–271
Povilaitis R Z, Robinson M S, van der Bogert C H, Hiesinger H, Meyer H M, Ostrach L R. 2018. Crater density differences: Exploring regional resurfacing, secondary crater populations, and crater saturation equilibrium on the moon. Planet Space Sci, 162: 41–51
Qiao L, Head J, Wilson L, Xiao L, Kreslavsky M, Dufek J. 2017. Ina pit crater on the Moon: Extrusion of waning-stage lava lake magmatic foam results in extremely young crater retention ages. Geology, 45: 455–458
Remane J, Bassett M G, Cowie J W, Gohrbandt K H, Lane H R, Michelsen O, Naiwen W. 1996. Revised guidelines for the establishment of global chronostratigraphic standards by the International Commission on Stratigraphy (ICS). Episodes, 19: 77–81
Richardson J E, Abramov O. 2020. Modeling the Formation of the lunar

upper megaregolith layer. Planet Sci J, 1: 2
Robbins S J. 2019. A new global database of lunar impact craters >1–2 km: 1. crater locations and sizes, comparisons with published databases, and global analysis. J Geophys Res-Planets, 124: 871–892
Sahijpal S, Goyal V. 2018. Thermal evolution of the early Moon. Meteorit Planet Scien, 53: 2193–2211
Salmon J, Canup R M. 2014. Accretion of the Moon from non-canonical discs. Phil Trans R Soc A, 372: 20130256
Salvador A. 2013. International Stratigraphic Guide. Boulder, Colorado: Geological Society of America
Schmitt H H, Trask N J, Shoemaker E M. 1967. Geologic map of the Copernicus quadrangle of the Moon, Miscellaneous Geologic Investigations. Flagstaff, Arizona: U.S. Geological Survey. Map I-515
Schultz P H, Crawford D A, Ambrose W A, Williams D A. 2011. Origin of nearside structural and geochemical anomalies on the Moon. In: Ambrose W A, Williams D A, eds. Recent Advances and Current Research Issues in Lunar Stratigraphy. McLean, Virginia: Geological Society of America. 141–159
Schultz P H, Crawford D A. 2016. Origin and implications of non-radial Imbrium Sculpture on the Moon. Nature, 535: 391–394
Scott D H, McCauley J F. 1977. Geologic map of the west side of the Moon, Geologic Atlas of the Moon. Flagstaff, Arizona: U.S. Geological Survey. I–1034
Shearer C K, Hess P C, Wieczorek M A, Pritchard M E, Parmentier E M, Borg L E, Longhi J, Elkins-Tanton L T, Neal C R, Antonenko I, Canup R M, Halliday A N, Grove T L, Hager B H, Lee D C, Wiechert U. 2006. Thermal and magmatic evolution of the moon. In: Jolliff B L, Wieczorek M A, Shearer C K, Neal C R, eds. New Views of the Moon. Chantilly, Virginia: The Mineralogical Society of America. 365–518
Shoemaker E M, Hackman R J. 1962. Stratigraphic basis for a lunar time scale. Symp-Int Astron Union, 14: 289–300
Shoemaker E M. 1964. The geology of the moon. Sci Am, 211: 38–47
Snape J F, Nemchin A A, Whitehouse M J, Merle R E, Hopkinson T, Anand M. 2019. The timing of basaltic volcanism at the Apollo landing sites. Geochim Cosmochim Acta, 266: 29–53
Snyder G A, Taylor L A, Halliday A N. 1995. Chronology and petrogenesis of the lunar highlands alkali suite: Cumulates from KREEP basalt crystallization. Geochim Cosmochim Acta, 59: 1185–1203
Stegman D R, Jellinek A M, Zatman S A, Baumgardner J R, Richards M A. 2003. An early lunar core dynamo driven by thermochemical mantle convection. Nature, 421: 143–146
Stoffler D, Ryder G, Ivanov B A, Artemieva N A, Cintala M J, Grieve R A F. 2006. Cratering history and lunar chronology. In: Jolliff B L, Wieczorek M A, Shearer C K, Neal C R, eds. New Views of the Moon. Chantilly, Virginia: Mineralogical Society of America. 519–596
Stöffler D, Ryder G. 2001. Stratigraphy and isotope ages of lunar geologic units: Chronological standard for the inner solar system. Space Sci Rev, 96: 9–54
Stuart-Alexander D E, Wilhelms D E. 1975. The Nectarian system, a new lunar time-stratigraphic unit. J Res U. S. Geol Surv, 3: 53–58
Taylor S R. 1989. Growth of planetary crusts. Tectonophysics, 161: 147–156
Terada K, Anand M, Sokol A K, Bischoff A, Sano Y. 2007. Cryptomare magmatism 4.35 Gyr ago recorded in lunar meteorite Kalahari 009. Nature, 450: 849–852
Wang Y, Wu B, Xue H, Li X, Ma J. 2021. An improved global catalog of lunar impact craters (≥1 km) with 3D morphometric information and updates on global crater analysis. J Geophys Res-Planets, 126: e2020JE006728
Warren P H. 1985. The magma ocean concept and lunar evolution. Annu Rev Earth Planet Sci, 13: 201–240
Weiss B P, Tikoo S M. 2014. The lunar dynamo. Science, 346: 1246753
Whitaker E A. 1981. The lunar Procellarum basin. Proc Lunar Planet Sci, 12: 105–111
White L F, Černok A, Darling J R, Whitehouse M J, Joy K H, Cayron C, Dunlop J, Tait K T, Anand M. 2020. Evidence of extensive lunar crust formation in impact melt sheets 4,330 Myr ago. Nat Astron, 4: 974–978
Whitten J L, Head J W. 2015. Lunar cryptomaria: Physical characteristics, distribution, and implications for ancient volcanism. Icarus, 247: 150–171
Wilhelms D E, McCauley J F, Trask N J. 1987. The Geologic History of the Moon. Washington DC: U.S. Government Printing Office
Wilhelms D E. 1970. Summary of lunar stratigraphy: Telescopic observations, Geological survey professional paper 599-F. Washington D.C.: U. S. Government Printing Office
Wood J A. 1975. Lunar petrogenesis in a well-stirred magma ocean. In: 6th Lunar and Planetary Science Conference. 6: 881–883
Yamamoto S, Nakamura R, Matsunaga T, Ogawa Y, Ishihara Y, Morota T, Hirata N, Ohtake M, Hiroi T, Yokota Y, Haruyama J. 2012. Massive layer of pure anorthosite on the Moon. Geophys Res Lett, 39: L13201
Yue Z, Michael G G, Di K, Liu J. 2017. Global survey of lunar wrinkle ridge formation times. Earth Planet Sci Lett, 477: 14–20
Yue Z, Yang M, Jia M, Michael G, Di K, Gou S, Liu J. 2020. Refined model age for Orientale Basin derived from zonal crater dating of its ejecta. Icarus, 346: 113804
Zhang B, Lin Y, Moser D E, Hao J, Shieh S R, Bouvier A. 2019. Imbrium age for zircons in Apollo 17 South Massif impact melt breccia 73155. J Geophys Res-Planets, 124: 3205–3218
Zhang F, Li C L, Zou Y L, Liu J Z, Liu J J, Zheng Y C, Miao L C, Wang S J, Lin Y T, Liu D Y, Ouyang Z Y. 2010. Lunar tectonic evolution: A conceptual basis for interpreting the lunar photographic images achieved by Chang'e 1 orbiter. Geochimica, 39: 110–122
Zhang N, Ding M, Zhu M H, Li H, Li H, Yue Z. 2022. Lunar compositional asymmetry explained by mantle overturn following the South Pole-Aitken impact. Nat Geosci, 15: 37–41
Zhu M H, Artemieva N, Morbidelli A, Yin Q Z, Becker H, Wünnemann K. 2019a. Reconstructing the late-accretion history of the Moon. Nature, 571: 226–229
Zhu M H, Wünnemann K, Artemieva N. 2017. Effects of Moon's thermal state on the impact basin ejecta distribution. Geophys Res Lett, 44: 11,292–11,300
Zhu M H, Wünnemann K, Potter R W K, Kleine T, Morbidelli A. 2019b. Are the Moon's nearside-farside asymmetries the result of a giant impact? J Geophys Res-Planets, 124: 2117–2140

(Editorial handling: Bing SHEN)